Nitrogen Cycling in Coastal Marine Environments
Edited by T. H. Blackburn and J. Sørensen

CHAPTER 13

Benthic Fauna and Biogeochemical Processes in Marine Sediments: The Role of Burrow Structures

ROBERT C. ALLER

13.1 INTRODUCTION

Most marine sediments underlying oxygenated bottom waters are either permanently or periodically inhabited by a variety of large, bottom-dwelling animals. These organisms transport particles and fluid during feeding, burrowing, tube construction and irrigation activity (Rhoads, 1974). As a result, surfi-

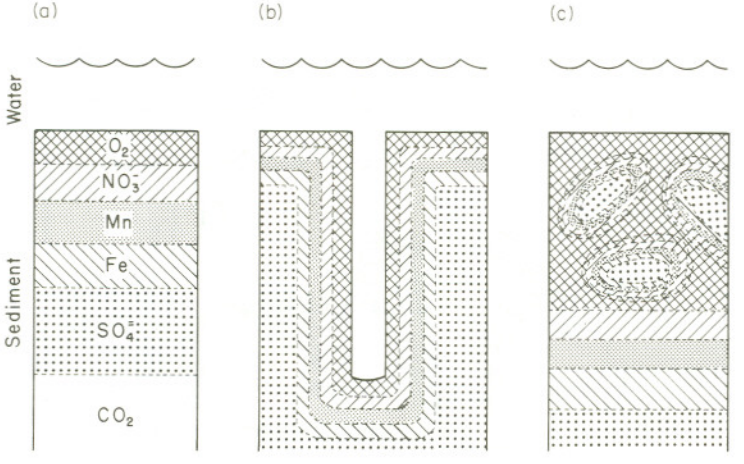

Figure 13.1. (a) Idealized, one-dimensional vertical succession of major oxidants associated with heterotrophic metabolism and diagenetic reactions of organic matter in marine sediments (see, for example, Froelich *et al.*, 1979; Berner, 1980). Vertical scaling depends on sedimentary environment. (b) Variation of diagenetic reaction geometry around cylindrical burrow microenvironment. (c) Spherical reaction distribution generated within fecal pellet aggregates. (After Aller, 1982.)

cial sedimentary deposits are transformed from bodies dominated by one-dimensional, vertical transport processes and diagenetic reaction distributions into bodies characterized by dynamic, three-dimensional mosaics of biogenic microenvironments (Figure 13.1). These structures and their creators significantly influence the bulk composition of a deposit, sedimentary solute profiles, reaction rate distributions and material fluxes across the sediment–water interface. The exact influence depends on the reaction kinetics governing a given chemical constituent, and on the particular configuration, scale and residence times of microenvironments. Tubes and burrows are the most important classes of structures in this respect, and their roles in determining biogeochemical properties of a deposit, especially the sedimentary nitrogen cycle, are emphasized here. More general reviews of the effects of macroorganisms on sediment diagenesis and particle reworking are given in Aller (1982), Fisher (1982), and Robbins (1985).

13.2 BURROW MICROENVIRONMENTS

Tubes and burrows are simply cyclindrical or ellipsoidal holes of varied complexity excavated for purposes of feeding or dwelling by animals inhabiting the seafloor. Depending on their mobility, infauna continually construct transient burrows of very short residence time (mobile fauna) or maintain relatively stable structures for longer periods (discretely mobile, sedentary fauna).

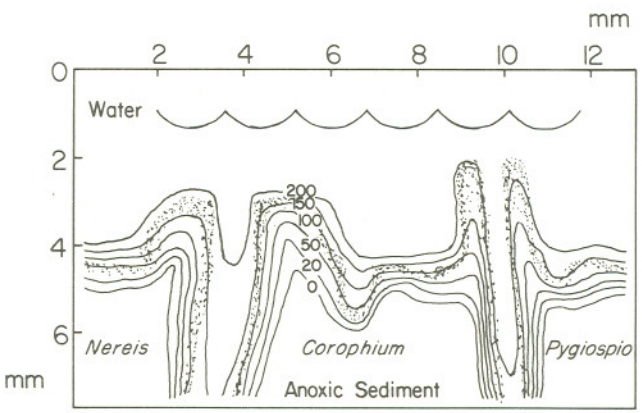

Figure 13.2. The injection of oxygen into sediments during irrigation activity is demonstrated quantitatively by the microscale distribution of oxygen concentrations near the sediment–water interface and around burrow structures of the polychaetes *Nereis* and *Pygiospio*, and part of a *Corophium* burrow (amphipod) in organic-rich muds. Contours in μM (μmol/liter). (After Jørgensen and Revsbech, 1985.)

At any given moment the seafloor is therefore a patchwork of tubes and burrows in various states of construction, maintenance and disrepair.

The central core of most burrows is usually irrigated with overlying water by the inhabitant. If the burrow wall is permeable to diffusion, solute concentration gradients are established between burrow water and surrounding sediment and diffusive transport occurs. Burrows formed in anoxic sediment, such as found commonly in nearshore or shelf environments, locally introduce oxygen into a deposit, increasing the total area of oxic–anoxic boundaries in addition to the surface available for diffusive exchange (Figure 13.2). This changes both the relative dominance and distribution of oxidation–reduction reactions such as NH_4^+, Mn^{2+}, Fe^{2+}, and HS^- oxidation, and increases biogeochemical heterogeneity. In contrast, actively irrigated burrows in oxic or suboxic sediment more

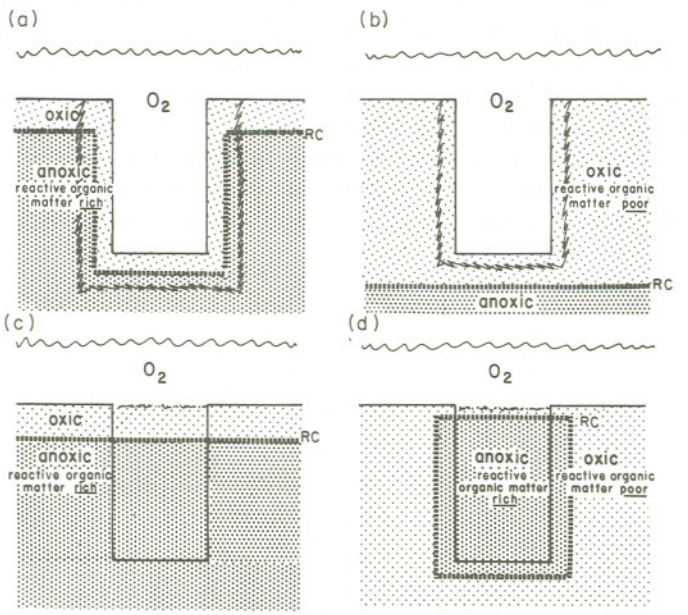

Figure 13.3. (A) Schematic representation of irrigated burrow embedded in anoxic sediment typical of nearshore environments. Region of elevated activity due to mucus secretions, organic-rich particles, and irrigation indicated by jagged line. (B) Irrigated burrow embedded in oxic or suboxic background typical of relatively organic-poor sediments such as in the deep sea. (C) Infilling of type A burrow with reactive sediment locally increases decomposition but decreases extent of oxic-anoxic boundary. (D) Infilling of type B burrow can create additional oxic–anoxic boundary due to anoxic pod embedded in oxic background. (After Aller and Aller, 1986.)

typical of the deep-sea (Grundmanis and Murray, 1982; Emerson *et al.*, 1980) probably do not dramatically alter the distribution of redox reactions.

The relative effect on redox heterogeneity in these two end-member cases can be reversed when reactive organic matter from the sediment–water interface fills in vacated burrows (Figure 13.3). In both instances a local increase in decomposition rates occurs in the burrow-fill relative to ambient sediment, due to input of reactive substrate (e.g. Skopintsev, 1981; Westrich and Berner, 1984). This increases the surface area of the oxic–anoxic boundary in the oxic sediment background and decreases it in the anoxic case (Figure 13.3). Under these circumstances the trapping of reactive material by burrow structues in an oxic or suboxic background can produce a nearly comparable effect on reaction distribution along the burrow wall–sediment boundary as an oxygenated burrow wall does in an anoxic background. Redox-sensitive metals such as Fe and Mn, solubilized during reduction and precipitated under oxidizing conditions, are often enriched along the oxic–anoxic boundary. Enrichment occurs on the inner side of the burrow wall in the irrigated burrow case and on the outer side in the infilled case (Figure 13.4). Mineral discontinuities of this kind provide a record of diffusion–reaction conditions in a deposit.

The zone immediately surrounding many tubes or burrows is often a site of elevated (2–3 ×) bacterial populations and metabolic activity compared to ambient sediment (Aller and Yingst, 1978; Henriksen *et al.*, 1983; Hylleberg, 1975;

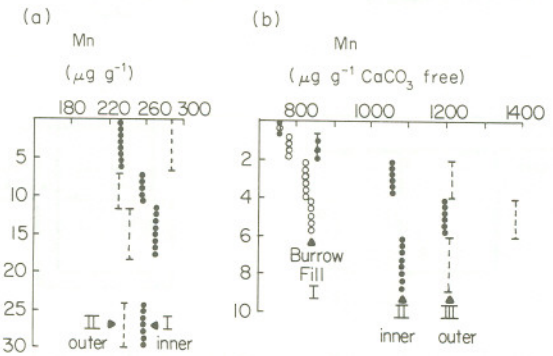

Figure 13.4. Distribution of solid phase Mn resulting from migrations around burrow structures like that of type A and B in Figure 12.3. (a) *Amphitrite ornata* burrow from Barnstable Harbor, Massachusetts, Mn enriched on inner wall of burrow. Ambient sediment averages 217 μg/g below 2 cm. (After Aller and Yingst, 1978.) (b) Infilled burrow from Nova Scotian Rise (~ 4830 m), Mn enriched on outer edge of burrow boundary. Ambient sediment averages 1100 μg/g below 2 cm. (After Aller and Aller, 1986.)

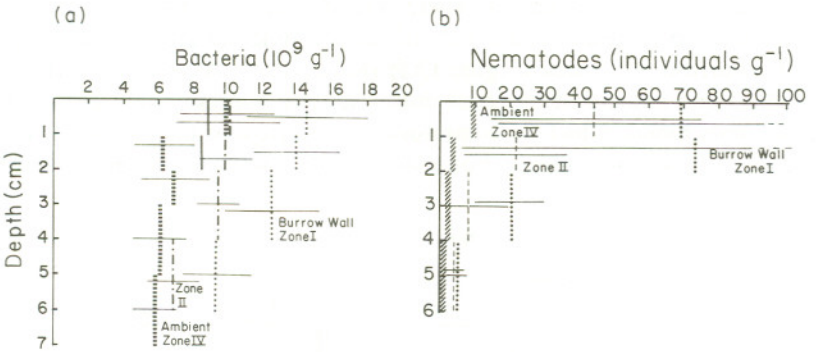

Figure 13.5. Burrows are often sites of enhanced bacteria and meiofaunal populations. (a) Average total numbers of bacteria around five open or vacated and infilled burrows from Nova Scotian Rise, western North Atlantic. Radial zones are ~ 1–1.5 cm successive annuli centered on the burrows at various depths. Ambient is average of numerous subcores taken away from burrows. (b) Average total number of nematodes corresponding to bacteria distributions in (a). (After Aller and Aller, 1986.)

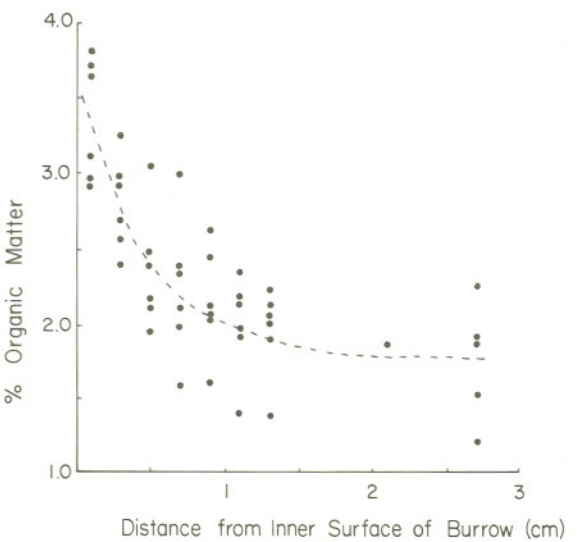

Figure 13.6. Burrow walls are commonly enriched with mucus secretions and small particles relative to surrounding sediments. In this case, distributions of total organic matter (loss on ignition, 500 °C) from six *Upogebia pugettensis* burrows in Bodega Bay, California indicate substantial mucus enrichment in the inner burrow wall. No measurable particle size variation occurs. (After Thompson, 1972.)

Kristensen *et al.*, 1985; Aller and Aller, 1986). Meiofaunal distributions are also altered, with absolute and relative abundances of different groups changing near specific burrow structures (Figure 13.5) (Reise, 1981; Aller and Aller, 1986). Biological and associated biogeochemical activity is presumably enhanced by organic enrichment which is common along burrow walls (Figure 13.6), the presence of the oxic–anoxic boundary which increases chemolithotrophic

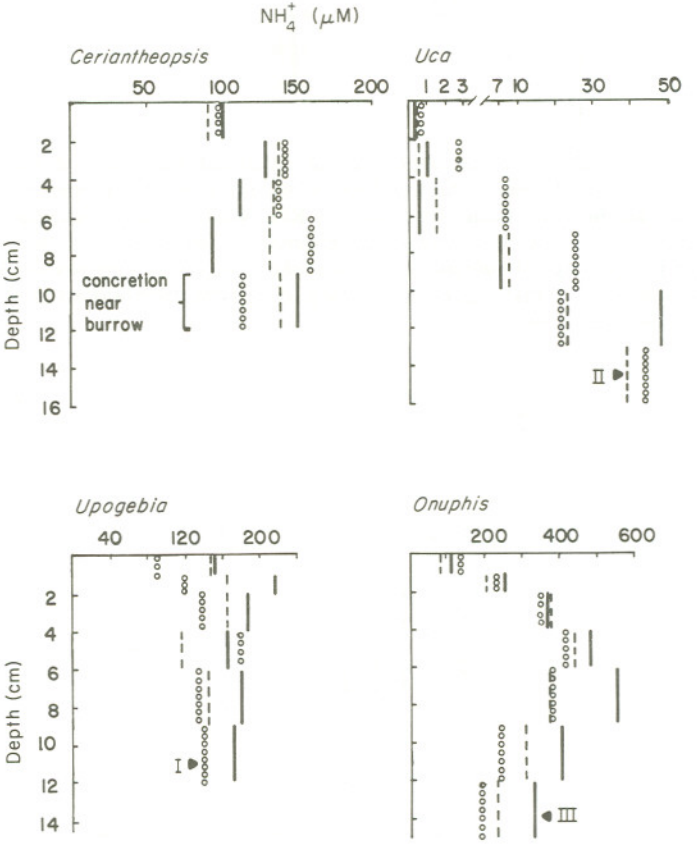

Figure 13.7. A three-dimensional variation in solute distributions exists around many burrows. Examples of NH_4^+ distributions near *Ceriantheopsis* (from Long Island Sound, Connecticut) *Uca*, *Upogebia* and *Onuphis* (North Inlet, South Carolina) illustrate a spectrum of distribution types with either elevated or depleted NH_4^+ concentrations found near the burrow relative to surrounding sediment. Zonal sampling centered on burrow axis in each case with Zone I, II and III = 0–3.5 cm, 3.5–6, 6–9 cm (*Ceriantheopsis*), 0–3.7, 3.7–8.9, 8.9–12 cm (*Uca*), and 0–3.7, 3.7–5.1, 5.1–8.9 cm (*Upogebia*; *Onuphis*). (After Aller, unpublished.)

activity, and the proximity to the irrigated burrow core which acts as a source for oxidants and a sink for potentially inhibitory metabolities.

The distribution of the products or reactants of organic matter decomposition in sediment near burrows reflects the diffusive source/sink property of the irrigated burrow cores, variation in metabolic activity around burrows, proximity to other microenvironments, and in some cases differences in diffusive permeability of the burrow wall or lining relative to surrounding sediment. The potential effects of several of these factors are illustrated by the distribution of porewater NH_4^+ concentrations around burrows formed by different species of infauna in nearshore anoxic muds (Figure 13.7). Gradients of generally increasing NH_4^+ toward the burrow axis are found around the examples *Ceriantheopsis* (burrowing anemone) and *Uca* (fiddler crab) burrows, while decreasing porewater NH_4^+ occurs around *Upogebia* (mud lobster) and *Onuphis* (onuphid polychaete). Increasing concentrations near burrows may be due to increased NH_4^+ production, or to a relatively impermeable burrow wall compared to other burrows within the deposit (Figure 13.8). The diffusive permeability of many burrow linings is ~ 2–$3\times$ lower than high-porosity muddy sediment ($\phi \sim 0.8$) for small inorganic solutes (Aller, 1983). In the case of *Ceriantheopsis*, the leathery burrow lining, while permeable to diffusion, is of sufficient thickness (~ 1–2 mm) and lower permeability than surrounding sediment, that an elevation of NH_4^+ near the burrow probably occurs due to local transport properties alone. This

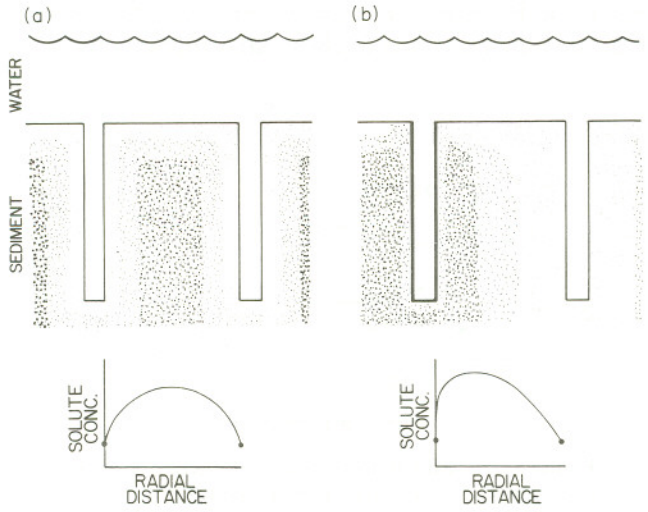

Figure 13.8. Apparent elevation of solutes such as NH_4^+ around a given burrow may be caused by impermeability of a burrow wall relative to other burrows in a deposit, rather than by elevated metabolic activity. (a) Equal permeability; (b) unequal permeability. (After Aller, 1983.)

interpretation is substantiated in the present case by $^{35}SO_4$-reduction rate measurements, which showed no significant radial variation near *Ceriantheopsis*. In contrast, increased NH_4^+ around *Uca* burrows, which lack a lining and have no evident wall cementation, is almost certainly due to increased production compared to surrounding sediment. A decrease in NH_4^+ near *Upogebia* burrows and *Onuphis* tubes presumably reflects loss of NH_4^+ by diffusion into the irrigated axis, or consumption during nitrification along the inner oxygenated burrow or tube walls, as discussed earlier. *Upogebia* burrow walls tend to be cemented and in this case had only a 10–20% lower diffusivity than ambient sediment.

In addition to the previously mentioned factors, the residence time of a burrow at a particular site in a deposit, together with the response time of a given chemical constituent or biological species, determines the patterns in chemical and biological properties around it. Because of the small diffusion scales involved, steady-state solute concentration gradients form quickly following burrow construction. Different constituents reach steady-state distributions over various time scales, however, due to differences in diffusion coefficients and reaction rates (e.g. Lerman, 1979). For example, solid-phase gradients in diagenetically mobile metals such as Fe and Mn often require relatively long times (several weeks) to be established, whereas porewater NH_4^+ distributions may be at steady state during much of the same period. This means that individual burrows, formed by members of the same species in the same deposit, may vary substantially in a variety of properties, due to residence time alone.

Because burrow walls often encompass the interface between oxic and anoxic sediments, they are important sites of chemolithotrophic activity such as NH_4^+

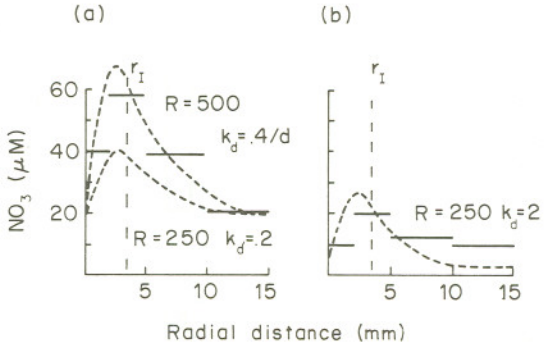

Figure 13.9. Radial distributions of interstitial NO_3^- near *Nereis virens* burrows demonstrate nitrification in a thin zone around the inner wall surface. (a) Burrows in sediment with organic C ~ 1%. (b) Burrows in sediment with organic C ~ 2%. (After Kristensen *et al.*, 1985.) Radial diffusion–reaction model fits as described in text, R = nitrification rate, μM/d; k_d = denitrification rate constant, 1/d

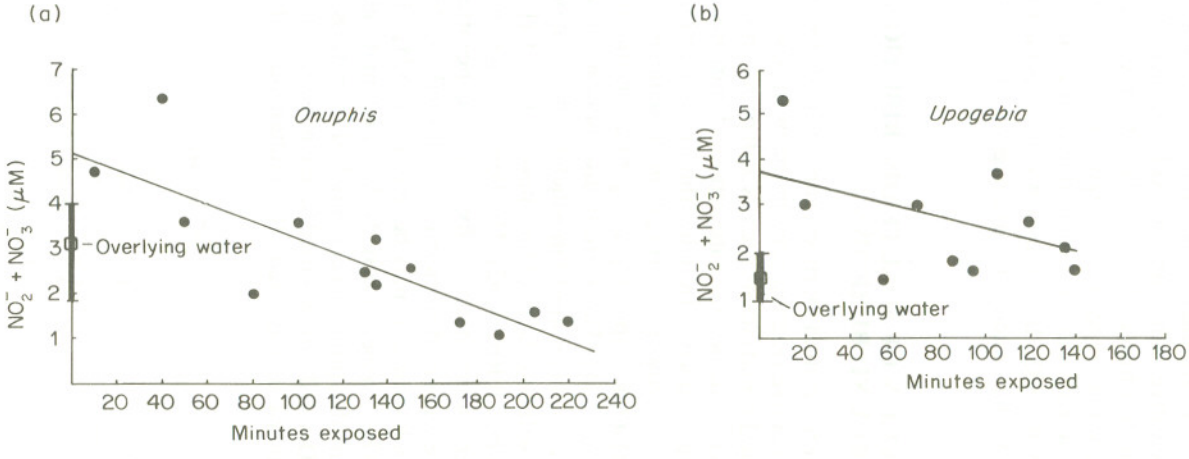

Figure 13.10. Despite irrigation, burrow water can differ in composition from overlying water due to diffusive interaction with surrounding sediment, intense metabolic activity in burrow walls and excretion from the burrow inhabitant. In this case, NO_3^- concentrations of water from burrows in a tidal flat (North Inlet, South Carolina) are shown as a function of time since irrigation (low tide). Initial elevated NO_3^- relative to overlying water demonstrates net nitrification during irrigation; the decrease following cessation of irrigation demonstrates the associated denitrification–nitrate reduction rate in the burrow wall and surrounding sediment. (a) *Onuphis* (polychaete) each point average of two to ten burrows; (b) *Upogebia* (mud lobster) each point one burrow. (After Aller *et al.*, 1983.)

and HS^- oxidation (Aller and Yingst, 1978; Henriksen *et al.*, 1983; Kristensen *et al.*, 1985). This is demonstrated directly by the distribution and concentrations of oxidation products such as NO_3^- around burrows (Figure 13.9). The properties of burrow water are also sensitive indicators of oxidation activity. Despite irrigation, burrow water often has lower pH, lower HCO_3^-, higher Fe^{2+}, and higher NO_3^- than overlying water, suggesting a significant nitrification and sulfide oxidation in the burrow wall and a substantial influence on the burrow habitat (Figure 13.10; Aller *et al.*, 1983). In sulfide-rich sediments burrow waters can take on properties similar to that of acid mine drainage on a microscale (Aller and Yingst, 1978).

13.3 QUANTIFICATION OF SOLUTE DISTRIBUTIONS AROUND BURROWS

Pore water solute distributions around burrows can be used, together with diffusion–reaction models, to derive reaction rates in the burrow wall, estimate solute fluxes and investigate additional factors such as wall permeability, burrow size and spacing, all of which influence the interaction of burrows and their inhabitants with surrounding sediments. Initially, the one-dimensional distribution of O_2 and NO_3^- around burrows and vertically in the sediment is modeled to demonstrate several important principles regarding diffusion and reactions in cylindrical geometries (Figure 13.11). The vertical distribution of NO_3^- in a deposit can be described by a two-layer model in which nitrification occurs at a constant rate R_n in a surface sediment layer of thickness, L_1 (Vanderborght and Billen, 1975; Jahnke *et al.*, 1982; Billen, 1982). The layer is taken as bounded above by a well-stirred water column having a fixed NO_3^- concentration, and below by a zone of nitrate reduction–denitrification. Although 10–50% of the NO_3^- consumed in organic-rich sediments may be reduced to NH_4^+ (Koike and Hattori, 1978; Sørensen, 1978; Kasper, 1983), N flux and material balance calculations indicate that denitrification must commonly dominate (Kemp *et al.*, 1982; Seitzinger *et al.*, 1984). Denitrification is used here synonymously with total nitrate reduction unless otherwise indicated. If simultaneous nitrification–

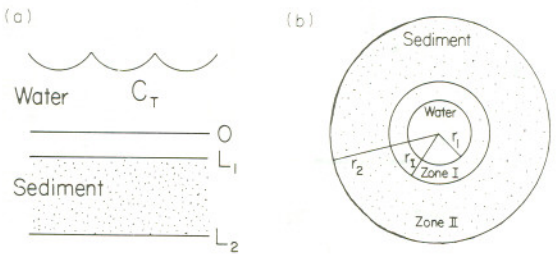

Figure 13.11. (a) One-dimensional vertical geometry used in composite planar model. (b) One-dimensional geometry used in composite radial model

denitrification is allowed in the nitrification zone, no qualitative conclusions are changed, although both total nitrification and denitrification must increase in such a case, in order to explain a given NO_3^- profile. Assuming production of NO_3^- at a rate independent of NO_3^- concentration (zero-order kinetics) and NO_3^- consumption in proportion to NO_3^- (first-order; Billen, 1978; Kaplan, 1983; Hattori, 1983), the steady-state vertical NO_3^- distribution is described by:

Nitrification:

$$\text{Layer 1,} \quad \frac{\partial C_1}{\partial t} = 0 = D_1 \frac{\partial^2 C_1}{\partial x^2} + R_n \tag{1a}$$

$$\text{Layer 2,} \quad \frac{\partial C_2}{\partial t} = 0 = D_2 \frac{\partial^2 C_2}{\partial x^2} - kC_2 \tag{1b}$$

Boundary conditions:

$$x = 0, \quad C_1 = C_T \tag{2a}$$

$$x = L_1, \quad C_1 = C_2 \tag{2b}$$

$$\phi_1 D_1 (\partial C_1 / \partial x) = \phi_2 D_2 (\partial C_2 / \partial x) \tag{2c}$$

$$x = L_2, \quad \partial C_2 / \partial x = 0 \tag{2d}$$

Where: x = space coordinate, positive into sediment;
t = time;
ϕ_1, ϕ_2 = porosity, layer 1, 2;
D_1, D_2 = solute diffusion coefficient, layer 1, 2;
C_1, C_2 = solute concentration, layer 1, 2.

Compaction is ignored, but different porosities and diffusion coefficients are allowed for easy adaptation to oxygen distributions and examination of the effects of burrow wall permeability on reactions. In the case of oxygen the origin of the coordinate system is fixed at the top of the viscous sublayer and L_1 corresponds to the sediment–water interface. The consumption of oxygen during heterotrophic decomposition of organic matter is essentially independent of O_2 (Focht and Verstraete, 1977; Skopintsev, 1981), but total consumption in sediments is strongly concentration-dependent, as demonstrated by sensitivity to the thickness of the boundary layer (Boynton *et al.*, 1981; Jørgensen and Revsbech, 1985). In this case, oxygen consumption is assumed first-order in oxygen concentration with a rate constant k_0.

A comparable two-zone model is assumed for radial distributions around burrows:

$$\text{Zone I} \quad \frac{\partial C_{\text{I}}}{\partial t} = 0 = \frac{D_{\text{I}}}{r}\left(\frac{\partial}{\partial r} r \frac{\partial C_{\text{I}}}{\partial r}\right) + R_n \tag{3a}$$

$$\text{Zone II} \quad \frac{\partial C_{\text{II}}}{\partial t} = 0 = \frac{D_{\text{II}}}{r}\left(\frac{\partial}{\partial r} r \frac{\partial C_{\text{II}}}{\partial r}\right) - kC_{\text{II}} \tag{3b}$$

Boundary conditions:

$$r = r_1, \quad C = C_T \tag{4a}$$

$$r = r_I, \quad C_I = C_{II} \tag{4b}$$

$$\phi_I D_I(\partial C_I/\partial r) = \phi_{II} D_{II}(\partial C_{II}/\partial r) \tag{4c}$$

$$r = r_2, \quad \partial C_{II}/\partial r = 0 \tag{4d}$$

with: r = radial coordinate, origin at burrow axis.

The outer boundary condition is equivalent to requiring that concentrations go through a maximum or minimum midway between any two burrows, or reach a constant value at some distance from the burrow. In both the vertical and radial models the lower or outer boundary condition is unimportant for large values of k(k_0 for O_2, k_d for NO_3^-). Solutions are given in the Appendix, for easy reference.

These models can be used to compare the relative vertical and radial penetration distances of O_2 into a deposit of fixed reduction reactivity, k_0. The standard conditions used in this and most subsequent models are $T = 22\,^\circ C$, salinity = 35‰, and sediment porosity $\phi = 0.85$. Whole sediment diffusion coefficients, D_s, are estimated from the free solution value, D, using the relation $D_s \sim \phi^2 D$ (Berner, 1980; Andrews and Bennett, 1981; Ullman and Aller, 1982). The free solution coefficient is calculated from the value at infinite dilution correcting for temperature and viscosity (Li and Gregory, 1974). For oxygen, $D = 1.75\,cm^2/d$ (Broecker and Peng, 1974). A non-reactive boundary layer 200 μm in thickness and $C_T = 230\,\mu M$ is assumed (Jørgensen and Revsbech, 1985).

The relative penetration depths of O_2 (5 μM level) into sediment with various values of k_0 are illustrated and compared with penetration depth around a burrow of radius 0.05 cm in Figure 13.12a. Typical reported vertical penetrations is nearshore muds are < 0.5 cm (Revsbech *et al.*, 1980; Jørgensen and Revsbech, 1985). The ratio of radial/planar penetration distance is plotted as a function of burrow radius at fixed values of k_0 in Figure 13.12 (L_2, r_2 large relative to $\sqrt{k_0/D_s}$). For identical sediment reactivity (k_0) the penetration distance is always less in the radial than planar case. In addition, the ratio of penetration distance is smaller at smaller burrow radii. This is a direct consequence of the low ratio of burrow surface (source) to surrounding sediment volume (sink) in a cylindrical geometry. These predicted relations are apparently substantiated by measured distributions, where O_2 concentration contours are compressed around burrows compared to the surface layer (Figure 13.2), although this could also be due to differences in k_0. Relative reactivity of the burrow wall and surface sediment can be compared directly in this way using O_2 penetration distances if diffusion coefficients are known.

The radial nitrification–nitrate reduction model can be used to fit the NO_3^- distributions around *Nereis* burrows measured by Kristensen *et al.* (1985) and calculated reaction rates compared with their estimates of potential nitrification

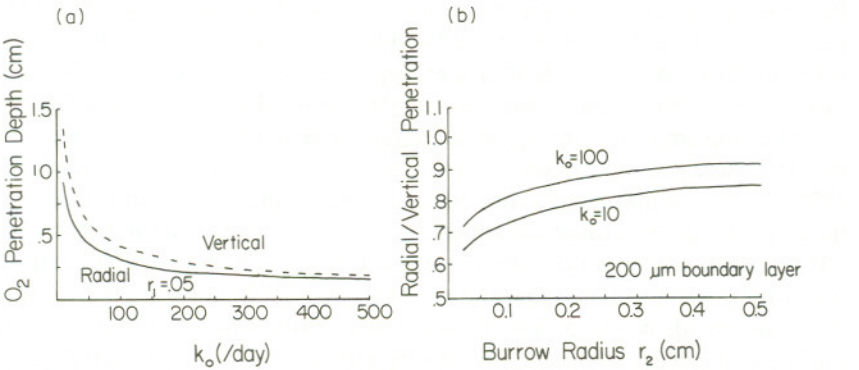

Figure 13.12. (a) Comparison of O_2 penetration distance from boundary as a function of rate constant k_0 for planar and radial geometries; viscous boundary layer = 200 μm. (b) Ratio of penetration distance for oxygen in radial and planar geometries as a function of burrow radius r_1 at fixed values of k_0 (1/d)

rates (Figure 13.9). These profiles were taken from burrows in a relatively organic poor ($\sim 1\% C$) (Figure 13.9a) and rich ($\sim 2\% C$) (Figure 13.9b) sediment background. In this case the *in situ* $T = 2.5\,^{\circ}$C, salinity = 19‰, and $\phi \sim 0.45$. Because $\phi < 0.7$, $D_s \sim \phi D$ (Ullman and Aller, 1982) so that $D_s \sim 0.399\,\text{cm}^2/\text{d}$. Taking the oxygenated nitrification zone to be 0.35 cm thick and the average burrow radii (r_1) to be 0.25 cm (based on an observed range 0.25–0.5 cm), and $r_2 = 2.3$ cm ($N = 600/\text{m}^2$), fits to the measured profiles are shown in Figure 13.9. The calculated *in situ* nitrification rates are $R \sim 500\,\mu$M/d (μmol/liter porewater/day) for the organic-poor sediment and $R \sim 250\,\mu$M/d for the organic-rich sediment. This compares with the estimate by Kristensen *et al.* (1985) of potential nitrification ~ 1300–$1700\,\mu$M/d made for both burrow types by correcting laboratory measurements at 22 °C to 2.5 °C ($Q_{10} \sim 2.5$). Potential nitrification rate estimates typically agree within a factor of ~ 2 with measured values (Henriksen *et al.*, 1981) so that differences found here are not necessarily unreasonable. Nitrate reduction–denitrification rate constants are $k_d = 0.4$/d and 2/d for the organic-poor and organic-rich sediments respectively. These are within the range expected for nearshore sediments of comparable organic content and grain size (Billen, 1978; Liu and Kaplan, 1984; Henriksen *et al.*, 1981). Models of radial profiles of this type are sensitive to estimates of burrow radius and nitrification zone thickness, so that great care must be taken in sampling these structures for estimation of rates. In addition, sampling should be done in either rings or radial sectors in order to properly average concentration distributions over finite intervals.

Although the radial model produces NO_3^- concentration profiles which are similar in shape to vertical profiles away from the oxygenated surficial interface, the radial diffusion–reaction geometry has different consequences for the relative

balance of nitrification–denitrification in sediments than does the planar geometry. This can be demonstrated by plotting the ratio of total denitrification/total nitrification for representative examples. Figure 13.13a shows the relative ratio when nitrification is fixed at a rate 300 μM/d in the oxygenated layer and the consumption rate, k_d, in surrounding sediment is taken as either 1/d or 10/d. These rates are reasonable for nearshore muds and muddy sands (Billen, 1978; Blackburn and Henriksen, 1983; Liu and Kaplan, 1984) and produce net fluxes in the general observed range (Nixon *et al.*, 1976; Klump and Martens, 1983). Other model values are: $r_1 = 0.1$ cm, $r_1 = 0.4$ cm ($r_1 - r_1 = 0.3$ cm), with variable r_2 for the radial model and $L_1 = 0.3$ cm; $L_2 > 2$ cm for the planar model. $D_s = 1.04\,\text{cm}^2/\text{d}$, $\phi = 0.85$, and $C_T = 10\,\mu$M in both cases. An additional plot illustrates the effect, at fixed k_d, of altering nitrification rate and overlying water nitrate concentration on the maximum possible ($r_2 > 2$) or saturation denitrification–nitrification ratio (Figure13.13b). When the saturation ratio is 1 there is no net flux of NO_3^- across the sediment–water interface; when it is > 1 the NO_3^- flux is into the sediment. These calculations demonstrate two important points: (1) the ratio of denitrification–nitrification in a cylindrical geometry is greater than in a comparable planar case having similar reaction rates and reaction zone thickness, and (2) the ratio changes rapidly as burrows come closer together and begin to interact ($r_2 = 1/\sqrt{\pi N}$ where $N =$ individuals/area). The implications of these differences for nitrogen cycling in bioturbated sediments are developed subsequently within the context of a more general

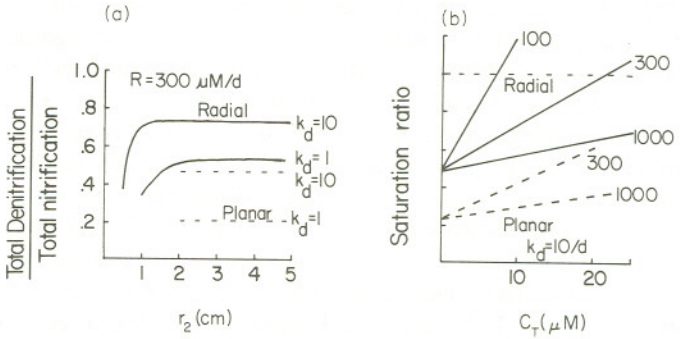

Figure 13.13. (a) Ratio of total denitrification to total nitrification in radial and planar models with identical reaction rates ($R = 300\,\mu$M/d, $k_d = 1, 10$) and thickness of nitrification layer (0.1 cm). Radial model is shown as a function of burrow spacing (r_2 to demonstrate interaction distance of burrows (ratio falls off) as function of k_d. (b) Ratio at maximum (i.e. $r_2 > 2$) as function of overlying water NO_3^- (C_T) and burrow wall nitrification rate. Radial geometry always results in a greater percentage of denitrification than does a planar diffusion geometry

model for bulk sediment composition and sediment–water exchange in the bioturbated zone.

13.4 THE AVERAGE MICROENVIRONMENTS AND BULK SEDIMENT DISTRIBUTIONS

It is possible to relate diffusion–reaction processes at the microenvironment scale to bulk sediment properties by postulating the existence of an average, or at least dominant, microenvironment. If the composition and behavior of the average microenvironment is known, then so is that of the sediment body. In the bioturbated zone the average functional microenvironment is assumed to be a hollow annulus comparable to a single burrow with its immediately surrounding sediment (Aller, 1980). From the standpoint of diffusion–reaction distributions the sediment is envisioned as functioning like a collection of such hollow cylinders packed together. This is an idealized description of a complex zone, but is relatively physically realistic and has proven robust in application to natural sediments (Aller, 1982). In the present case the average microenvironment is taken as a composite, or coaxial, hollow cylinder in order to differentiate reactions such as nitrification and diffusion in the burrow wall (zone I) from surrounding sediment (zone II) (Figure 13.14). This essentially adds together the planar and radial models discussed previously. To simply mathematics, nitrification in Zone II is given a decay term that is exponential with depth in the deposit so that nitrate production goes to zero at some finite depth below the upper interface and away from the burrow. This permits nitrification to dominate near the upper interface and denitrification to dominate in deeper regions. It avoids the likely but mathematically complicated two-layer nitrification–denitrification distribution in both the vertical and horizontal dimensions.

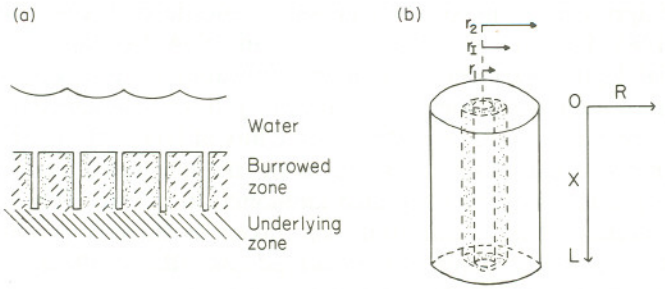

Figure 13.14. (a) Vertical cross-section of bioturbated sediment with idealized average burrow distribution. (b) Single hollow composite zone cylinder of sediment visualized as the average functional microenvironment in the burrowed zone. Dimensions and reference frame correspond to those of the transport–reaction model in the text

The equations describing the steady state distribution of a solute in such a microenvironment are:

$$\text{Zone I:} \quad \frac{\partial C_{\mathrm{I}}}{\partial t} = 0 = D_{\mathrm{I}} \frac{\partial^2 C_{\mathrm{I}}}{\partial x^2} + \frac{D_{\mathrm{I}}}{r}\left(\frac{\partial}{\partial r} r \frac{\partial C_{\mathrm{I}}}{\partial r}\right) + R_{\mathrm{I}} \tag{5a}$$

$$\text{Zone II:} \quad \frac{\partial C_{\mathrm{II}}}{\partial t} = 0 = D_{\mathrm{II}} \frac{\partial^2 C_{\mathrm{II}}}{\partial x^2} + \frac{D_{\mathrm{II}}}{r}\left(\frac{\partial}{\partial r} r \frac{\partial C_{\mathrm{II}}}{\partial r}\right) + R_{\mathrm{II}} \tag{5b}$$

where:

t = time;
x = vertical space coordinate, origin at sediment–water interface, positive into sediment;
r = radial coordinate measured from cylinder axis;
$C(x, r, t)$ = porewater solute concentration mass/volume porewater;
$D_{\mathrm{I}}, D_{\mathrm{II}}$ = bulk diffusion coefficient in zones I and II respectively
$\phi_{\mathrm{I,\,II}}$ = porosity in sones I and II
$R_{\mathrm{I}}, R_{\mathrm{II}}$ = reaction term in zones I and II

The region below the burrow zone is controlled by one-dimensional vertical diffusion and reaction distributions. Compaction is ignored and adsorption is not included because only steady-state distributions are considered (Berner, 1980).

For the present purposes, reaction terms for each zone are taken as:

$$R = R_n^{\mathrm{I}} + R_1^{\mathrm{I}} - k_C^{\mathrm{I}} \tag{6a}$$

$$R_{\mathrm{II}} = R_1^{\mathrm{II}} + R_0^{\mathrm{II}} \exp(-\alpha x) - k_{\mathrm{d}}^{\mathrm{II}} + R_n^{\mathrm{II}} \exp(-\beta x) \tag{6b}$$

The terms R_n^{I} and $R_n^{\mathrm{II}} \exp(-\beta x)$ represent zero-th-order nitrification rates in the burrow wall and surface sediment respectively. R_1^{I}, R_1^{II}, and $R_0^{\mathrm{II}} \exp(-\alpha x)$ are zero-th-order ammonium production rates, and $k_{\mathrm{d}}^{\mathrm{I}}$ and $k_{\mathrm{d}}^{\mathrm{II}}$ are first-order denitrification (includes nitrate reduction) rate constants. These are good analytical approximations for the reaction kinetics in each case (Billen, 1978; Kaplan, 1983; Hattori, 1983; Liu and Kaplan, 1984; Skopintsev, 1981). The exponential depth-dependent function for nitrification in zone II is assumed for mathematical simplicity as mentioned previously. It is also assumed that the only limit on nitrification is the total steady-state flux of NH_4^+ into the nitrification zone so that in a completely balanced model the integrated nitrification rate cannot be greater than the integrated ammonification rate. This differs from previous models where nitrification was taken as directly proportional to ammonification at each depth in the oxidized zone (Billen, 1982).

Boundary conditions on the cylinder microenvironment are:

Zone I: (oxidized burrow wall, $r_1 \leqslant r \leqslant r_{\mathrm{I}}$)

$$x = 0, \quad C_{\mathrm{I}} = C_T \tag{7a}$$

$$x = L, \quad \partial C_{\mathrm{I}}/\partial x = B_{\mathrm{I}} \tag{7b}$$

$$r = r_1, \quad C_{\mathrm{I}} = C_T \tag{7c}$$

$$r = r_1, \quad C_I = C_{II} \tag{7d}$$
$$, \quad \phi_I D_I(\partial C_I/\partial r) = \phi_{II} D_{II}(\partial C_{II}/\partial r) \tag{7e}$$

Zone II: (sediment around burrow wall, $r_1 \leqslant r \leqslant r_2$)

$$x = 0, \quad C_{II} = C_T \tag{8a}$$
$$x = L, \quad \partial C_{II}/\partial x = B_{II} \tag{8b}$$
$$r = r_1, \quad C_I = C_{II} \tag{8c}$$
$$\phi_I D_I(\partial C_I/\partial r) = \phi_{II} D_{II}(\partial C_{II}/\partial r) \tag{8d}$$
$$r = r_2, \quad \partial C_{II}/\partial r = 0 \tag{8e}$$

These correspond to a constant solute concentration, C_T, at the sediment–water interface and in the burrow (7a, 8a), flux continuity across the base of the burrowed zone (7a, 8b), flux and concentration continuity between the inner burrow wall and surrounding sediment (7c, 7d; 8c, 8d), and that solute distributions reach a maximum or minimum (or constant value) midway (or some distance r_2) between any two burrows (8e). In the case of conditions (7b) and (8b), only a single measured value of $\partial C/\partial x = B$ is available in practice below the bioturbated region. It is assumed that $B_{II} = (\phi_s D_s B/\phi_{II} D_{II}) = B$, $B_I = (\phi_{II} D_{II} B/\phi_I D_I)$, and that the diffusion coefficient D_s and ϕ_s at $x > L$ are the as in zone II. The solutions to equations (5) and (6) with conditions (7) and (8) are given in the Appendix.

Concentration distributions in the microenvironment are translated into average vertical concentrations equivalent to measured pore water profiles, $\bar{C}$, by integrating the concentrations in zones I and II over finite vertical intervals x_1 to x_2 and weighting the respective zones by volumes:

$$\bar{C} = \frac{\pi r_1^2 L}{V_T} C_T + \frac{V_I 2\pi \int_{x_1}^{x_2}\int_{r_1}^{r_1} C_I r\,dr\,dx}{V_T 2\pi \int_{x_1}^{x_2}\int_{r_1}^{r_2} r\,dr\,dx} + \frac{V_{II} 2\pi \int_{x_1}^{x_2}\int_{r_1}^{r_2} C_{II} r\,dr\,dx}{V_T 2\pi \int_{x_1}^{x_2}\int_{r_1}^{r_2} r\,dr\,dx} \tag{9}$$

where: $V_I = \pi(r_1^2 - r_1^2)(x_2 - x_1)$
$V_{II} = \pi(r_2^2 - r_1^2)(x_2 - x_1)$
$V_T = \pi r_2^2$

The flux, J, across the sediment–water interface is given by:

$$J = -\frac{\phi_I D_I A_I 2\pi \int_{r_1}^{r_1} \left(\frac{\partial C_I}{\partial x}\right)_o r\,dr}{A_T 2\pi \int_{r_1}^{r_1} r\,dr} - \frac{\phi_{II} D_{II} A_{II} 2\pi \int_{r_1}^{r_2} \left(\frac{\partial C_{II}}{\partial x}\right)_o r\,dr}{A_T 2\pi \int_{r_1}^{r_2} r\,dr} \tag{10}$$

where: $A_I = \pi(r_1^2 - r_1^2)$
$A_{II} = \pi(r_2^2 - r_1^2)$
$A_T = \pi r_2^2$

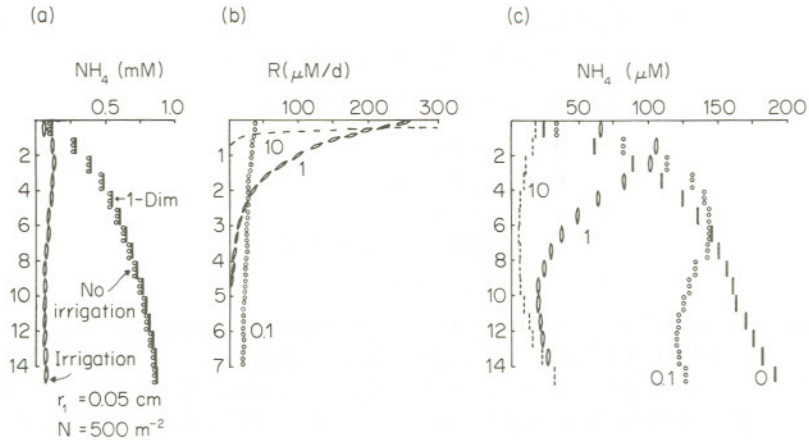

Figure 13.15. (a) Average vertical distributions of NH_4^+ in sediment predicted by a one-dimensional vertical diffusion–reaction model, a cylinder model with stagnant burrow water and the cylinder model with irrigated burrows. Burrows are taken as 1 mm diameter with $500/m^2$ ($r_2 = 2.52$ cm), other values as in case 1, Table 13.1. (b) Reaction distributions for NH_4^+ with identical integrated rates (flux) in top 15 cm but different depth-dependent attenuations of 0.1, 1 and 10/cm. Note vertical scale change. (c) Average NH_4^+ distributions in sediments with fixed diffusion geometry $r_1 = 0.05$ cm, $N = 500\,m^2$ but with variable reaction rate distributions as in (b). Attenuation of O represents constant production with depth ($R = 17.6\,\mu M/d$). The total NH_4^+ flux out of the sediment is the same in each case.

The effect of burrow construction and irrigation on the build-up patterns of NH_4^+ in sediments is illustrated in Figure 13.15 for the reasonable case where $N = 500$ burrows/m^2 ($r_2 = 2.52$ cm) and $r_1 = 0.05$ cm. There is no nitrification along the surficial sediment or burrow interfaces in this example. Comparison is shown between irrigated burrows, burrows but no irrigation (stagnant), and a one-dimensional model ($r_2 \to \infty$; $r_1 \to 0$). Model values (Table 13.1; case 1) correspond to a station from Mud Bay, South Carolina, a shallow estuarine embayment on the southeast coast of the United States (Aller, 1980). The profile marked 'no-irrigation' was calculated using the basic burrow microenvironment model but allowing for stagnant burrow water that can vary from C_T in composition (Aller, 1984). When irrigation does not occur, burrow water quickly takes on the composition of surrounding sediment (Waslenchuk *et al.*, 1983; Kristensen, 1984; Aller *et al.*, 1983) and the sediment body is dominated at steady state by one-dimensional diffusion except at extremely high burrow densities or low porosities (Aller, 1984). These profiles demonstrate that a relatively few irrigated burrows at natural sizes and abundances can have major effects on the build-up patterns of constituents such as NH_4^+ which are produced at essentially a constant rate (zero-th-order reactions).

Table 13.1. Microenvironment Model Values

	Case 1: NH_4^+	Case 2: NO_3^-
C_T	0.2 μM	variable
B	11 μM/cm	0
D_s	1.08 cm^2/d	1.04 cm^2/d
ϕ_s	0.85	0.85
α	0.61/cm	—
R_0^{II}	126 μM/d	—
R_1^{II}	3.9 μM/d	—
β	—	10
R_n^{II}	—	300 μM/d
R_n^I	—	variable
R_1^I	—	—
k_d^I	—	0
k_d^{II}	—	variable

The effect of burrows on NH_4^+ profiles depends strongly on the depth dependence of reaction rates; that is, the interaction between diffusion geometry and reaction rate distribution. Figure 13.15 illustrates NH_4^+ distributions that would result when the attenuation of NH_4^+ production with depth differs (α changes) but the total production rate (0–15 cm) or NH_4^+ flux out of the sediment is held constant ($\phi_s \int_0^L R dx$ = constant) at the Mud Bay rate of 2.24 n mol m^{-2} d^{-1} (other model values as in case 1, Table 13.1). Attenuation can differ in natural sediments due to changes in supply of reactive organic matter, sedimentation rate or mixing rate. The lower the attenuation ($\alpha \rightarrow 0$) the more the overall shape is similar to a one-dimensional profile. Note that the concentration gradient at the sediment–water interface becomes smaller when $\alpha \rightarrow$ large or $\alpha \rightarrow$ small, so that estimations of diffusive flux using a one-dimensional model of Fick's Law: $J = -\phi_s(\partial C/\partial x)_0$ become less accurate in each instance.

The ratio of the flux of NH_4^+ out of the bottom due to the measured vertical gradient (J_x) relative to the total flux is shown as a function of burrow abundance and radius in Figure 13.16 with R as in Figure 13.15 ($\alpha = 0.61$). This indicates the proportion of NH_4^+ escaping the sediment radially through burrow walls relative to that escaping by vertical diffusion. It is a direct estimate of the deviation of the measured flux (by incubation chambers, for example) from the predicted flux based on the porewater profile using a one-dimensional form of Fick's Law (see Aller, 1980 for detailed discussion).

Bulk concentration profiles of NH_4^+ are generally changed imperceptibly by burrow wall nitrification at typical reported rates of R_n (e.g. Kaplan, 1983) in organic-rich muds where nitrification layers are restricted ($\leqslant 0.5$ cm). Substantial changes may occur in sands where nitrification dominates a thicker zone of the deposit (Billen, 1982). In contrast, the NH_4^+ flux from the sediment and its pattern

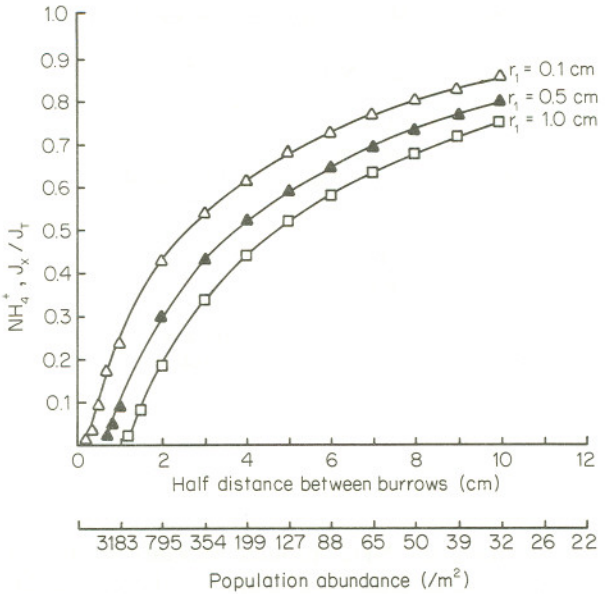

Figure 13.16. Ratio of the flux of NH_4^+ escaping across the upper sediment surface (exclusive of burrow water) to total NH_4^+ flux (vertical and radial diffusion) into burrows. As number and size of burrows increase a larger proportion of NH_4^+ produced in sediment escapes through burrow walls. No nitrification occurs in this case (case 1, Table 13.1, variable r_1, r_2)

of escape can be greatly complicated by nitrification along burrow walls and surficial sediment. The total flux of NH_4^+ is decreased by the total nitrification rate along both oxidized interfaces, and the geometry of NH_4^+ escape from the sediment can be completely altered from that depicted in Figure 13.16, depending on relative nitrification rates in the burrow wall and sediment surface. This must be determined in any given case and is of greatest significance in deposits poor in reactive organic matter.

Total nitrification per unit area of the bottom in a burrowed sediment (assuming an average burrow microenvironment) is given by:

$$\Sigma NO_3 = \phi_s \int_0^{L_1} R_n(x)dx + NL\phi_s 2\pi \int_{r_1}^{r_1} R_n(r)rdr$$

where:
N = burrows/unit area;
L = burrow length;
L_1 = surface nitrification layer depth;
$R_n(x)$, $R_n(r)$ = nitrification rates in surface sediment burrow wall.

In reality, of course, the second term is the sum over all the numbers, lengths, sizes and reaction rates in the various burrows present in a deposit. If for further simplicity $R_n(x) = R_n(r) = R_n$ is constant then the total nitrification taking place in a burrowed deposit relative to an unburrowed deposit is given by:

$$\frac{\Sigma\,NO_3 \text{ burrowed}}{\Sigma\,NO_3 \text{ no burrows}} = 1 + NL\pi(r_1^2 - r_1^2)/L_1$$

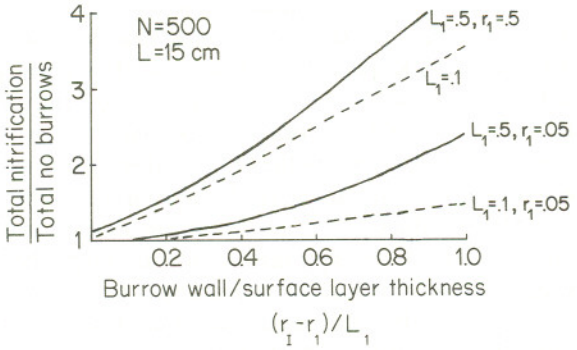

Figure 13.17. Ratio of total nitrification in a sediment with burrows to that with no burrows as a function of burrow wall nitrification layer to surficial sediment layer thickness. Burrow number is fixed at $N = 500$ and r_1 is varied in these examples. The nitrification ratio is a linear function of N and L (burrow length)

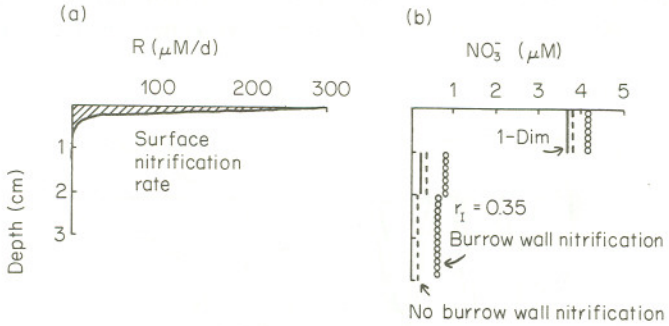

Figure 13.18. (a) Nitrification rate function assumed for surface sediment ($R_n = 300\exp(-10x)\,\mu$M/d). (b) Average NO_3^- distributions in sediment predicted by one-dimensional models, burrows with no nitrification ($r_1 = 0.05$ cm, $N = 500/m^2$ ($r_2 = 2.52$)), and burrows with a 3 mm thick nitrification zone (300 μM/d). The concentrations between 2 and 4 cm for the cases with burrows present would extend to the base of the burrowed zone (case 2, Table 13.1)

This relation is plotted in Figure 13.17. It illustrates the role of burrows in increasing total nitrification in a deposit (Henriksen *et al.*, 1980, 1983; Blackburn and Henriksen, 1983; Sayama and Kurihara, 1983; Kristensen *et al.*, 1985) and also illustrates the important role of radial geometry in determining the particular dependence. Total nitrification rate is not directly proportional to burrow surface area (inner wall) as it is for the upper sediment surface (planar) because of the dependence on $r_1^2 - r_1^2$.

Burrow wall nitrification has only a small effect on NO_3^- porewater distributions at most likely natural abundances when k_d, the denitrification rate constant, is relatively large: $\sim$ 1–20/d, as occurs in nearshore muds and muddy sands (Billen, 1978; Liu and Kaplan, 1984; Aller *et al.*, 1985). The profiles shown in Figure 13.18, for example, with $r_1 = 0.05$ cm, $r_1 - r_1 = 0.3$ cm, and $N = 500/m^2$, compared with $r_1 - r_1 = 0$ and the one-dimensional case, would be almost indistinguishable in practice; although the burrowed sediment with burrow wall nitrification would show a small NO_3^- background to the depth of the bioturbated zone. Model values ($T = 22\,°C$) are those of case 2 in Table 13.1 with $D_I = D_{II} = D_s$ and $k_d = 10$/d. Exceptions occur at extremely high infaunal abundances when burrow nitrification zones begin to coalesce into a single contiguous layer (Figure 13.19; after Henriksen *et al.*, 1983) or when k_d is small and oxidized zones large relative to burrow spacing.

Despite the lack of obvious impact on NO_3^- porewater profiles for many realistic burrow sizes and abundances, the presence of burrows with or without burrow wall nitrification can have dramatic effects on the total magnitude of the NO_3^- flux, the direction of NO_3^- flux, total denitrification and the relative ratios of denitrification to nitrification in a deposit. The exact effects depend on the rate of nitrification in the oxidized layer, the denitrification rate constant, k_d, in surrounding sediment, the thickness of the oxidized zones, the length and radius

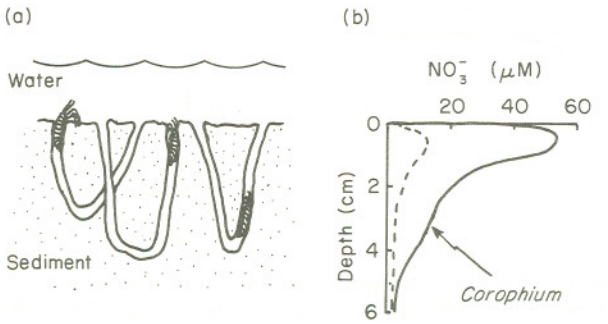

Figure 13.19. At high abundances burrow nitrification can significantly alter NO_3^- porewater distributions relative to sediments lacking macrofauna. In this case *Corophium* is present at $\sim 3000/m^2$ so that burrow wall nitrification zones become nearly contiguous. (After Henriksen *et al.*, 1983.)

of burrows present, the number of burrows, and the overlying water NO_3^- concentration. Some of these relationships are illustrated here theoretically, using rates, burrow sizes and abundances likely to be characteristic of many nearshore muddy environments. It is important to recognize in these examples that nitrification within sediments is generally the primary source of NO_3^- for denitrification; therefore the two processes are necessarily coupled and influenced by diffusion geometry. Diffusion coefficients are assumed to be the same in the burrow wall and ambient sediment (case 2, Table 13.1) and unless otherwise indicated nitrification is taken as 300 μM/d in the reactive burrow wall and $300\exp(-10x)$ in surface sediment (as in Figure 13.18). Simultaneous nitrification–denitrification in the burrow wall is not considered in these examples ($k_d^I = 0$; $k_d^{II} = k_d$) although it may occur (e.g. Hattori, 1983; Jenkins and Kemp, 1984). As in the previous one-dimensional examples, no qualitative conclusions are changed by its inclusion.

In the absence of burrow wall nitrification, the flux of NO_3^- into a reducing sediment ($k_d > 0$) is always increased by the presence of irrigated burrows compared with unburrowed sediment. This occurs because of the concentration-dependent kinetics of NO_3^- reduction (first-order) and the increased NO_3^- supply by irrigation. It is accentuated by the radial diffusion geometry because of the high reducing sediment volume burrow wall to surface area. If k_d is sufficiently large and nitrification rate in surficial sediment low enough, the sign of the total NO_3^- flux can be reversed so that the deposit is a net sink for NO_3^-. As the rate of burrow wall nitrification and/or thickness of the wall increases, total nitrification and the NO_3^- flux can change accordingly, with large

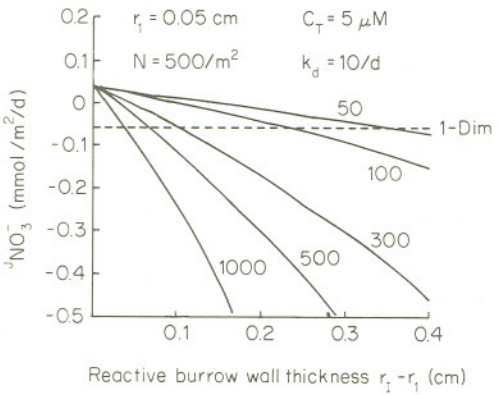

Figure 13.20. The net flux of NO_3^- across the sediment–water interface depends strongly on burrow wall thickness and nitrification rate. Nitrification rates vary in this case between 50 and 1000 μM/d; $C_T = 5\ \mu$M; $k_d = 10$/d; other model values as in case 2, Table 13.1

increases in NO_3^- flux out of the sediment. This is illustrated in Figure 13.20 for the case of fixed size and abundance of burrows and in Figure 13.21 for variable numbers of burrows, radii and nitrification zone thickness. The total flux can potentially increase by factors of 10–20 above the one-dimensional case, and the direction of the flux is a very strong function of burrow wall thickness, overlying water concentration, and k_d. These changes are not simply proportional to sediment surface area increase as shown by the magnitude, sign and nonlinear behavior of fluxes relative to burrow abundance (burrows interact as determined by scaling distances of $\sqrt{k_d/D_s}$, r_1 and r_l).

Although these calculations are done for the steady-state case, they also demonstrate the expected time dependence of newly burrowed sediment. If, for example, infauna were added experimentally to organic-rich sediment, the initial effect might be to increase the NO_3^- flux into a deposit (for example, $r_l - r_1 = 0.1$ line in Figure 13.21), but if the oxidized zone around the burrow grows, the flux can reverse direction (change, for example, to $r_l - r_1 = 0.3$ line in Figure 13.21) or stabilize at any given value at or below the initial line, depending on the quantity of reactive organic matter in surrounding sediment. A similar relative relationship should occur between mobile benthos (thin oxidized zone, short burrow residence time) and sedentary benthos (possible thick oxidized zone, long burrow

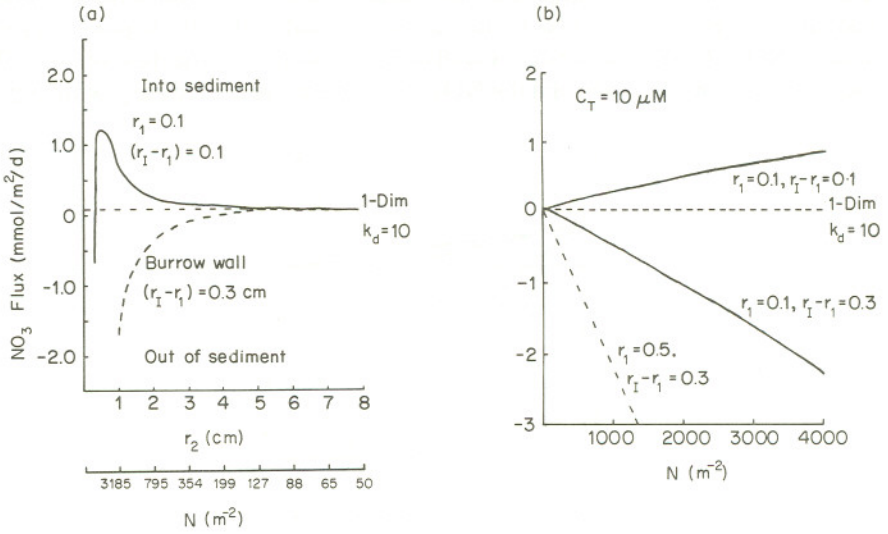

Figure 13.21. The net flux of NO_3^- across the sediment–water interface can be increased, decreased and change sign as a result of infauna, depending on burrow radius (r_1), nitrification zone thickness ($r_l - r_1$), and burrow abundance. (a) Flux relative to r_2 (interburrow distance) and N with $k_d = 1/d$. (b) Flux relative to burrow abundance (N) with $k_d = 10/d$. The one-dimensional prediction is shown as the horizontal dashed line in each case. Other values as in case 2, Table 13.1

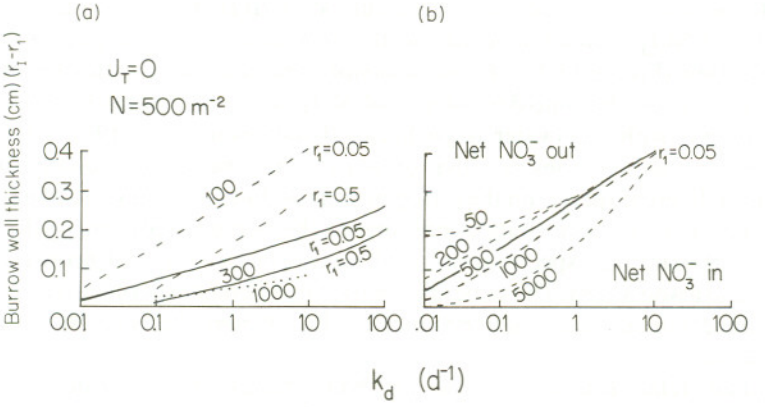

Figure 13.22. (a) Relationship of burrow wall thickness, k_d of surrounding sediment, nitrification rate (100–1000 μM/d) in burrow wall, and burrow radius required to produce a zero net flux of NO_3^- across the burrow wall (radial model of Figure 13.11b). For a given curve, values in the field above the curve produce a net radial flux out of the sediment around the burrow, values below produce a net flux in (N-500/m^2). (b) Relationship as in (a) but at fixed $r_1 = 0.05$ cm and variable interburrow distances ($N = 50$–5000/m^2)

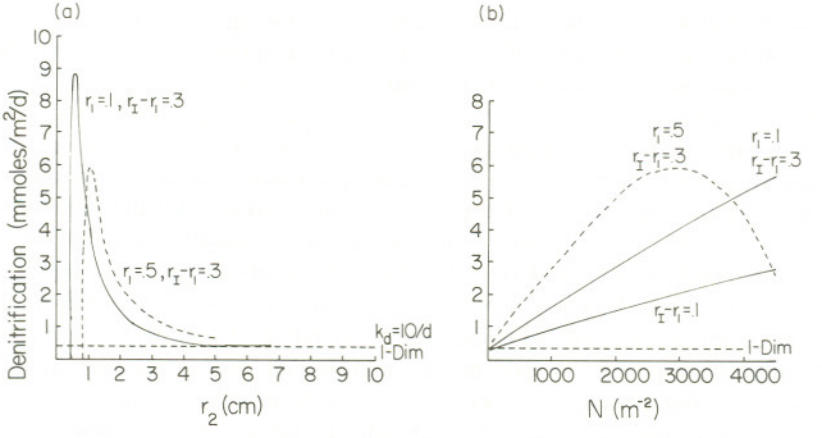

Figure 13.23. (a) Total denitrification rate in burrowed zone ($L = 15$ cm) as function of interburrow distance r_2 and burrow radius r_1. Burrow nitrification zone fixed at $r_1 - r_1 = 0.3$ cm in thickness. (b) Total denitrification as function of N (linear scale), r_1, and nitrification zone thickness ($r_1 - r_1$). Optimal abundances (for maximum denitrification) with $r_1 = 0.1$ cm lie offscale. Total denitrification in the one-dimensional case represented by horizontal line (model values case 2, Table 13.1)

residence time). There are also a large number of likely natural states where the net flux of NO_3^- across the burrow wall is very close to zero despite substantial nitrification (Figure 13.22). These behaviors are consistent with experimental observations on the time-dependence of NO_3^- fluxes in laboratory microcosm experiments with freshwater oligochaetes (Chatarpaul *et al.*, 1979, 1980). The calculations also demonstrate that great care must be taken in comparing the effects of different species on the nitrogen cycle as differences in sizes, abundances and transient or steady-state conditions of the burrow–sediment system may readily obscure true species-specific differences in burrow wall properties and microbial associations. The same species used in different experiments at different abundances or size (age) could produce totally different effects on NO_3^- flux and nitrification.

Similar relationships to those for NO_3^- fluxes are illustrated for total denitrification (includes nitrate reduction) in burrowed relative to unburrowed sediments in Figure 13.23. Total denitrification increases dramatically (up to 10–20 × the one-dimensional value) as burrows are added to the sediment, with the largest increases occurring the thicker the burrow nitrification zone. As burrows pack closer together, the zone of denitrification reaches an optimal size relative to the NO_3^- source and denitrification becomes maximal. Further increase in the number of burrows decreases the interburrow distance below the optimum, which depends on r_1, $r_l - r_1$, and k_d, and there is a lowering of total denitrification. Over most natural ranges of abundances and expected burrow radii, however, denitrification is still increased above the one-dimensional case, regardless of whether the maximum increase is obtained. These trends are due to the competing dependences of total denitrification on the magnitude of the NO_3^- source (increases with increasing C_T and $r_l - r_1$) and the volume of sediment in which denitrification occurs (decreases with increasing $r_l - r_1$).

Not only are both nitrification and denitrification generally increased by the presence of irrigated burrows, but the relative balance between the two reactions can be significantly altered (Figure 13.24). The ratio of total denitrification to total nitrification in burrowed sediment can be increased, decreased or unaffected, depending on burrow size, abundance, k_d (reactive organic reductant), and nitrification zone thickness. For example, small burrows with a thin oxidized zone (1 mm) can be expected to increase the denitrification–nitrification ratio at abundances less than $\sim 3000/m^2$ in organic-rich muds, whereas somewhat smaller numbers of large burrows ($r_1 = 0.5$ cm) should decrease the ratio. It seems likely that in many organic-rich muds with relatively small burrows (1–3 mm diameter) and moderate populations of benthos ($\sim 1000/m^2$), the major effect is to increase the relative ratio of denitrification–nitrification. Burrow wall thickness also plays an important role in this balance, as does nitrification rate (Figure 13.24). This again emphasizes the different behavior with respect to nitrogen cycling that must occur between recently colonized areas (transient) and stable communities (steady state) or between mobile (small burrow residence

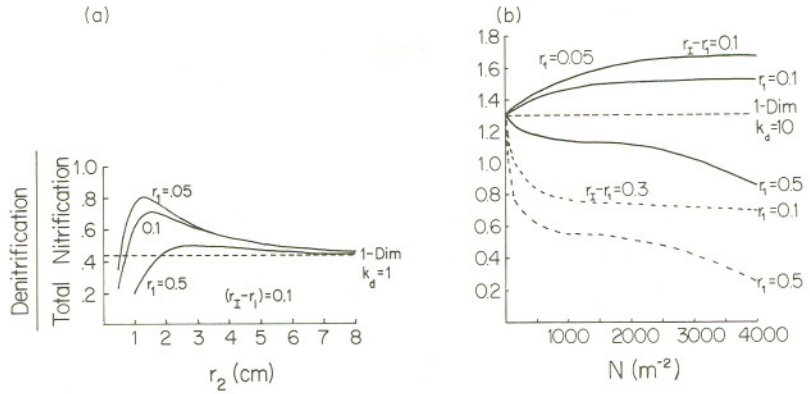

Figure 13.24. (a) Ratio of total denitrification to nitrification as function of burrow radii and spacing at fixed reactive wall thickness. This ratio in addition to total denitrification is often increased above the one-dimensional prediction ($k_d = 1/d$). (b) Ratio of denitrification to total nitrification as function of burrow radii, abundance, and wall thickness $(r_I - r_1) = 0.1$ (solid lines), $r_I - r_1 = 0.3$ (dashed). Note that even when the ratio is decreased below the one-dimensional level, total denitrification can still be much greater than for a stratified sediment (compare Figure 13.23b, $r_1 = 0.1$, $r_I - r_1 = 0.3$). Other model values as in case 2, Table 13.1

time) and sedentary populations (long residence time, possible thicker oxidized burrow wall zone) or even between juvenile and adult populations (size differences) of the same species. Experiments to compare effects of different species and their influence on the total nitrogen cycle must be carefully designed with these facts in mind, making appropriate allowances for differences in size, abundance and any departures from steady-state conditions. These relationships are further complicated by true species-specific effects such as burrow wall construction and diffusivity which can also alter the relative balance (Figure 13.25); although in most cases diffusivity effects are probably of minor importance for small inorganic solutes.

Overall, macrobenthos increase total denitrification and for likely natural situations also increase the ratio of denitrification to total nitrification. This implies that there have been systematic changes in the nitrogen cycle through geologic time. As biogenic reworking and burrowing depth increased in the early Paleozoic (Thayer, 1983), a greater proportion of the total remineralized nitrogen in the sea floor must have been denitrified and lost to nearshore ecosystems. It also raises the possibility that unlike constituents such as $Si(OH)_4$ which are recycled to plankton in overlying water more efficiently by the activities of marcrobenthos, the total return of available nitrogen may be decreased. This assumes that the relative balance between nitrate reduction and denitrification is

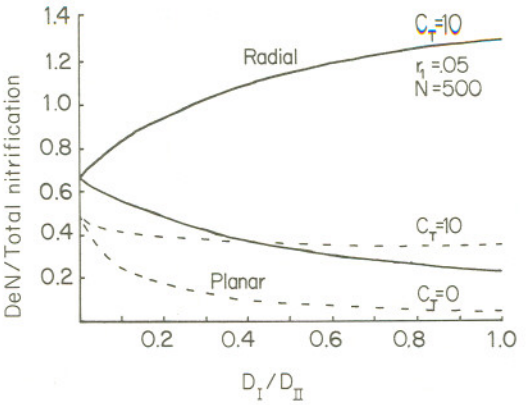

Figure 13.25. Burrow wall permeability can also affect the ratio of denitrification/total nitrification taking place around a burrow. The radial and planar models of Figure 12.11 are compared here for $C_T = 0$, 10 μM and L_1, $r_1 - r_1 = 0.1$ cm to demonstrate different sensitivities of radial and planar geometries to this effect. Most burrow walls would be expected to only slightly inhibit diffusion of small inorganic ions relative to surrounding sediment

not significantly changed by macrobenthos (Sørensen, 1978, Koike and Hattori, 1978).

13.5 SOURCE–SINK MODELS OF BULK CHEMISTRY OF THE BIOTURBATED ZONE

For many constituents it is possible to describe the effects of irrigated burrows on bulk sediment chemistry and sediment flux using a simple source–sink function, rather than the mathematically more complicated microenvironment description (Emerson *et al.*, 1984: Boudreau, 1984). This function is the form, $\eta(C - C_T)$ where η is a constant determined by the particular diffusion geometry of the sediment and the diffusion coefficient of the solute. In this way the simple one-dimensional mathematical formulation for diffusion–reaction distributions in the sediment is retained with inclusion of the source–sink function. In addition, the single parameter η allows ready comparison between different bottom areas in terms of overall macrobenthic influence on transport (Emerson *et al.*, 1984). The value of η necessary to mimic the average behavior of the microenvironment model can be used in both non-steady-state and steady-state cases and, in many instances, once a single value of η is found the value for other solutes can be calculated by multiplying the measured η by the ratio of respective solute diffusion coefficients (Aller and Yingst, 1985). The general relationship of η for

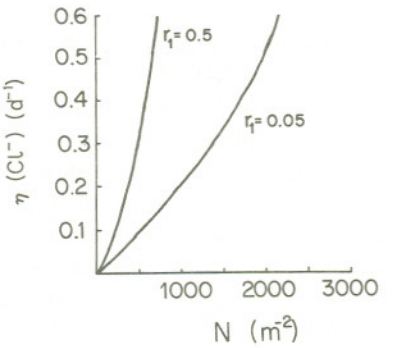

Figure 13.26. Relation of non-local source–sink parameter η for Cl^- in high-porosity mud ($\phi = 0.83$) compared to geometry of the cylinder microenvironment which would produce the same effect on bulk sediment composition

Cl^- to the geometric dimensions of the average microenvironment model is illustrated in Figure 13.26. This type of model is extremely useful in describing, for example, average NH_4^+ distributions in bioturbated deposits, but does not readily describe the effects of boundary reactions such as burrow wall nitrification, and interactions such as denitrification/nitrification balances resulting from specific geometries.

13.6 SEDIMENT AMMONIUM PRODUCTION RATES AND FLUXES

Although the fundamental limit on NH_4^+ production is the nature and quantity of reactive organic matter delivered to the sea floor, there is considerable evidence that in addition to increasing total nitrification and denitrification rates in sediment, burrow formation and irrigation stimulates sedimentary NH_4^+ production rates by at least ~ 20–30% relative to sediment uninhabited by macrofauna (Aller, 1978; Hyllebergn and Henriksen, 1980; Henriksen *et al.*, 1983; Aller and Yingst, 1985; Matisoff *et al.*, 1985). It is not known to what extent the total time-integrated production of NH_4^+ is increased ($\int_0^\infty R dt$ as opposed to R at some particular time t^*). Such increased production could offset, to some degree, increased loss of nitrogen to the planktonic community due to elevated denitrification, at least over short periods. This increase is distinct from direct excretion by macrofauna which may account for up to ~ 20–60% (usually $\sim 20\%$) of the total NH_4^+ flux from the sea floor under certain circumstances (Blackburn and Henriksen, 1983). (Many estimates of excretion flux contribution

may be overestimates due to the methods used of extracting animals from their natural burrows during incubation (Kristensen, 1983, 1984).) It is also distinct from the *non-steady-state* increase in NH_4^+ flux (or any other flux) from sediments which results when animals are initially added to or colonize a deposit. Part of this stimulation may result from physical mixing of sediment as burrows are constructed or particles manipulated during feeding. The breaking-down of aggregates in such cases may expose new substrate, fragment large particles and open stagnant port space (Greenwood, 1968; Stefanson, 1972; Hargrave, 1970; Aller, 1982). Injection of mucus into the deposit and grazing of bacteria during feeding may also stimulate microorganisms (Hargrave, 1976; Hargrave and Phillips, 1977; Yingst and Rhoads, 1980). These mechanisms require immediate contact of the animal with the sediment, and should occur only in the inhabited zone, particularly burrow walls as noted previously.

The relative build-up of interstitial NH_4^+ in aquaria experiments with single species demonstrate that stimulation of NH_4^+ takes place in bulk sediment away from burrows and in sediment below the bioturbated zone (Aller, 1978; Hylleberg and Henriksen, 1980; Henriksen *et al.*, 1980, 1983; Aller and Yingst, 1985). This suggests that transport of inhibitory metabolites, or in some instances supply of oxidants during irrigation, may be a major cause of stimulation. In this regard, many experiments on the effect of sediment mixing on reaction rates also resuspend the sediments into a larger volume of water, thereby simultaneously diluting the porewater (e.g. Kaspar, 1982; Blackburn and Henriksen, 1983; Bowden, 1984). When experiments which differentiate between mixing and build-up of metabolites are performed using an anoxic diffusion cell technique or mixed tank sediments there is often, but not always, a substantial increase in NH_4^+ production the more 'open' the decomposing sediment regardless of mixing (Aller and Yingst, 1985; Aller and Mackin, unpublished). If sediment irrigation affects NH_4^+ production in the manner described it is not entirely correct to describe its reaction rate as a zero-th-order function independent of concentration. The effect is apparently sufficiently small, however, that for many purposes it can be ignored.

13.7 CONCLUSIONS

Bioturbated marine sediments are mosaics of biogenic microenvironments, the most important of which are burrow structures. When irrigated with oxygenated overlying water by their inhabitants, burrows can produce major changes in the distribution of reactions, the rate of reactions and the build-up or depletion of reaction products or reactants in a deposit. Oxidation–reduction reactions are particularly influenced because irrigated burrows in anoxic sediments and infilled vacated burrows in oxic–suboxic sediments often result in extensions of the sea floor oxic–anoxic boundary. Burrow walls are sites of intense chemolithotrophic activity coupled to oxidation of reduced constituents such as HS^-, NH_4^+, and

Mn^{2+}. Metals such as Fe and Mn, which are mobilized along the redoxcline, are reprecipitated and concentrated near burrow walls. Partly as a result of the chemolithotrophic activity, partly due to injection of mucus secretions and selection of organic-rich small particles during burrow wall construction, and partly due to irrigation which removes inhibitory metabolites and supplies oxidants, burrow walls are zones of enhanced microbial and meiofaunal activity generally.

The distribution of solutes around burrows and the relative balance between reactions is strongly affected by the radial diffusion geometry, particularly in burrows of small radius. Oxygen penetrates about 70–80% as far into sediments around burrows as at the surficial sediment–water interface for the same sediment reactivity. A higher proportion of NO_3^- released by nitrification in the burrow wall is denitrified in adjacent sediment than in a planar geometry of otherwise equivalent reaction rates.

Oxygenated burrows increase the overall rate of nitrification in a deposit because they add sites of nitrification and stimulate bacterial activity. The influence of burrows on the flux of NO_3^- into or out of the sediment is a strong function of burrow radius, oxidized wall thickness, burrow spacing, and the first-order denitrification rate constant, k_d, in surrounding sediment (proportional to reactive organic matter/sediment volume). The smaller the burrow radius, thinner the burrow wall, and larger k_d, the more likely burrows increase the NO_3^- flux into a deposit despite increased nitrification. For a wide range of likely conditions in burrowed sediments, the net flux of NO_3^- can be close to zero.

As expected for a first-order concentration-dependent reaction, and because of increased nitrification, denitrification (includes nitrate reduction) is greatly increased by the presence of burrows unless the nitrification zones actually directly coalesce. For a given nitrification rate, burrow radius and wall thickness there is an optimal spacing of burrows to produce a maximal increase in denitrification. This demonstrates directly that surface area increase by burrows in a deposit is not necessarily an indication of their influence on reactions. Not only is total denitrification increased but the relative balance between denitrification and nitrification is altered by burrows. Depending again on radius, nitrification rate and zone thickness, and burrow spacing, the denitrification–nitrification ratio can increase or decrease. Many likely natural configurations of burrows in organic-rich muds where NH_4^+ production is highest should result in major ($\sim 2\times$) increases in this ratio. In addition to the increase in total denitrification this raises the interesting possibility that the sedimentary nitrogen cycle may have undergone major changes through geologic time with increased total and relative denitrification accompanying increased bioturbation as benthic communities developed. Unlike other constituents such as $Si(OH)_4$, the total flux to overlying planktonic communities of available nitrogen (NH_4^+, NO_3^-) remineralized on the sea floor probably is decreased by biogenic reworking and irrigation, due to increased production of N_2. This conclusion

assumes that total remineralization (time-integrated) of organic matter is not greatly different in the presence of macrobenthos as in their absence (total organic decomposition is zero-order in oxidants) although rates may differ at any given time.

Because of the strong dependence simply on burrow radius and abundance, great care must be taken in trying to derive species-specific effects on the nitrogen cycle from experiments. Major differences can result from size and abundance alone. Non-steady-state effects during burrow wall development, and differences between mobile and sedentary benthos, are likely for these reasons.

The effect of irrigated burrows on average build-up or depletion of constituents in sediments can be accounted for in a first-order source–sink function and constant parameter, η. This allows easy comparison of different communities in terms of their overall effect on transport and many reactions, but does not allow examination of detailed interaction between at least partly spatially separated reactions such as nitrification and denitrification, or diffusion properties of burrow walls.

In addition to direct excretion of NH_4^+, and in some cases non-steady-state alteration of sediment–water fluxes, macrobenthos apparently increase the rate of NH_4^+ production by ~ 20–30% in bulk sediment away from immediate burrow walls. The exact reason is not well understood, but may be related in part to a lower build-up of inhibitory metabolites in irrigated sediments. Interaction of macrobenthos with sedimentary reactions generally remains an understudied research area.

ACKNOWLEDGEMENTS

I thank J. Y. Aller, W. J. Ullman and J. E. Mackin for many stimulating discussions and aid in the field and laboratory over the years. J. E. Mackin was a codeveloper of the general composite cylinder model used to examine the nitrogen cycle in this chapter, and provided helpful comments on the manuscript. J. Westrich kindly performed the $^{35}SO_4$-reduction rate measurements around the *Ceriantheopsis* burrow. L. Jasper, A. Ray and J. Pasdeloup aided in manuscript preparation.

APPENDIX

The solutions to equations (1a, b) with boundary conditions (2a–d) are:

$$C_1(x) = C_T + Ax - \frac{R_n x^2}{2D_1}$$

$$C_2(x) = B\cosh(\sigma(x - L_2))$$

where: $\sigma = \sqrt{k/D_2}$

$$A = \left[\frac{R_n L_1}{D_1} (\cosh(\sigma(L_1 - L_2))) - \left(\frac{R_n L_1^2}{2D_1} - C_T \right) \times \frac{\phi_2 D_2}{\phi_1 D_1} \sigma \sinh(\sigma(L_1 - L_2)) \right] \Big/ \Delta$$

$$B = \left[C_T + \frac{R_n L_1^2}{2D_1} \right] \Big/ \Delta$$

$$\Delta = \cosh(\sigma(L_1 - L_2)) - \frac{\phi_2 D_2}{\phi_1 D_1} \sigma L_1 \sinh(\sigma(L_1 - L_2))$$

The solutions to equations (3a, b) with boundary conditions (3a–d) are:

$$C_{\mathrm{I}}(r) = C_T + A \log(r/r_1) + R_n(r_1^2 - r^2)/(4D_{\mathrm{I}})$$
$$C_{\mathrm{II}}(r) = B U_0(\mu r)$$

where: $\mu = \sqrt{k/D_{\mathrm{II}}}$

$$U_0(\mu r) = K_1(\mu r_2)\mathrm{I}_0(\mu r) + \mathrm{I}_1(\mu r_2) K_0(\mu r)$$

$$A = \left[\frac{r_{\mathrm{I}} R_n}{2D_{\mathrm{I}}} U_0(\mu r_1) - \frac{\phi_{\mathrm{II}} D_{\mathrm{II}}}{\phi_{\mathrm{I}} D_{\mathrm{I}}} \mu U_0'(\mu r_1) \left(\frac{R_n(r_{\mathrm{I}}^2 - r_1^2)}{4D_{\mathrm{I}}} - C_T \right) \right] \Big/ \Delta$$

$$B = \left[\frac{r_{\mathrm{I}} R_n}{2D_{\mathrm{I}}} \log(r_{\mathrm{I}}/r_1) + \frac{1}{r_{\mathrm{I}}} \left(C_T - \frac{R_n(r_{\mathrm{I}}^2 - r_1^2)}{4D_{\mathrm{I}}} \right) \right] \Big/ \Delta$$

$$U_0'(\mu r_{\mathrm{I}}) = K_1(\mu r_2)\mathrm{I}_1(\mu r_{\mathrm{I}}) - \mathrm{I}_1(\mu r_2) K_1(\mu r_{\mathrm{I}})$$

$$\Delta = \frac{\phi_{\mathrm{II}} D_{\mathrm{II}}}{\phi_{\mathrm{I}} D_{\mathrm{I}}} \mu U_0'(\mu r_{\mathrm{I}}) \log(r_1/r_{\mathrm{I}}) + U_0(\mu r_{\mathrm{I}})/r_{\mathrm{I}}$$

The solutions to equations (5a, b) with conditions (6ab), (7a–e) and (8a–e) are:

$$C_{\mathrm{I}}(x,r) = C_T + B_{\mathrm{I}} x - \sum_{n=0}^{\infty} \frac{2B_{\mathrm{I}}(-1)^n}{L\lambda_n^2} \frac{\mathrm{I}_0(\mu_n^{\mathrm{I}} r)}{\mathrm{I}_0(\mu_n^{\mathrm{I}} r_1)} \sin(\lambda_n x)$$
$$+ \sum_{n=0}^{\infty} \frac{G_n^{\mathrm{I}}}{(\mu_n^{\mathrm{I}})^2} \left(\frac{\mathrm{I}_0(\mu_n^{\mathrm{I}} r)}{\mathrm{I}_0(\mu_n^{\mathrm{I}} r_1)} - 1 \right) \sin(\lambda_n x)$$
$$+ \sum_{n=0}^{\infty} A_n U_{\mathrm{I}}(\mu_n^{\mathrm{I}} r) \sin(\lambda_n x)$$

$$C_{\mathrm{II}}(x,r) = C_T + B_{\mathrm{II}} x + \sum_{n=0}^{\infty} \left[B_n U_{\mathrm{II}}(\mu_n^{\mathrm{II}} r) - \frac{G_n^{\mathrm{II}}}{(\mu_n^{\mathrm{II}})^2} \right] \sin(\lambda_n x)$$

where: $\lambda_n = (n + \frac{1}{2})\frac{\pi}{L}, \quad n = 0, 1, 2, \ldots$

$$\mu_n^{\mathrm{I}} = \sqrt{\frac{k_d^{\mathrm{I}}}{D_{\mathrm{I}}} + \lambda_n^2}$$

$$\mu_n^{\mathrm{II}} = \sqrt{\frac{k_d^{\mathrm{II}}}{D_{\mathrm{II}}} + \lambda_n^2}$$

$$U_{\mathrm{I}}(\mu_n^{\mathrm{I}} r) = \mathrm{I}_0(\mu_n^{\mathrm{I}} r_1) K_0(\mu_n^{\mathrm{I}} r) - K_0(\mu_n^{\mathrm{I}} r_1) \mathrm{I}_0(\mu_n^{\mathrm{I}} r)$$

$$U_{\mathrm{II}}(\mu_n^{\mathrm{II}} r) = K_1(\mu_n^{\mathrm{II}} r_2) \mathrm{I}_0(\mu_n^{\mathrm{II}} r) + \mathrm{I}_1(\mu_n^{\mathrm{II}} r_2) K_0(\mu_n^{\mathrm{II}} r)$$

$$G_n^{\mathrm{I}} = \frac{2}{LD_{\mathrm{I}}}\left[\frac{k_d^{\mathrm{II}} C_T - R_N^{\mathrm{I}} - R_1^{\mathrm{I}}}{\lambda_n} + \frac{(-1)^n k_d^{\mathrm{I}} B_{\mathrm{I}}}{\lambda_n^2}\right]$$

$$G_n^{\mathrm{II}} = \frac{2}{LD_{\mathrm{II}}}\left[\frac{k_d^{\mathrm{II}} C_T - R_1^{\mathrm{II}}}{\lambda_n} + \frac{(-1)^n k_d^{\mathrm{II}} B_{\mathrm{II}}}{\lambda_n^2} + \frac{R_0(\alpha e^{-\alpha L}(-1)^n - \lambda_n)}{\alpha^2 + \lambda_n^2} + \frac{R_N(\beta e^{-\beta L}(-1)^n - \lambda_n)}{\beta^2 + \lambda_n^2}\right]$$

$$A_n = \left[U_{\mathrm{II}}(\mu_n^{\mathrm{II}} r_1) M_n \mu_n^{\mathrm{I}} \mathrm{I}_1(\mu_n^{\mathrm{I}} r_1) - \frac{\phi_{\mathrm{II}} D_{\mathrm{II}}}{\phi_{\mathrm{I}} D_{\mathrm{I}}} U'_{\mathrm{II}}(\mu_n^{\mathrm{II}} r_1) M_n \mathrm{I}_0(\mu_n^{\mathrm{I}} r_1) + N_n \mathrm{I}_0(\mu_n^{\mathrm{I}} r_1)\right] \Big/ \Delta_n$$

$$B_n = [M_n(U_{\mathrm{I}}(\mu_n^{\mathrm{I}} r_1)\mu_n^{\mathrm{I}} \mathrm{I}_1(\mu_n^{\mathrm{I}} r_1) - U'_{\mathrm{I}}(\mu_n^{\mathrm{I}} r_1)\mathrm{I}_0(\mu_n^{\mathrm{I}} r_1)) + N_n \mathrm{I}_0(\mu_n^{\mathrm{I}} r_1)]/\Delta_n$$

$$M_n = \left(\frac{2B_{\mathrm{I}}(-1)^n}{L\lambda_n^2} - \frac{G_n^{\mathrm{I}}}{(\mu_n^{\mathrm{I}})^2}\right)$$

$$N_n = \left(\frac{G_n^{\mathrm{I}}}{(\mu_n^{\mathrm{I}})^2} - \frac{G_n^{\mathrm{II}}}{(\mu_n^{\mathrm{II}})^2}\right)$$

$$U'_{\mathrm{I}}(\mu_n^{\mathrm{I}} r_1) = -\mu_n^{\mathrm{I}}(\mathrm{I}_0(\mu_n^{\mathrm{I}} r_1) K_1(\mu_n^{\mathrm{I}} r_1) + K_0(\mu_n^{\mathrm{I}} r_1)\mathrm{I}_1(\mu_n^{\mathrm{I}} r_1))$$

$$U'_{\mathrm{II}}(\mu_n^{\mathrm{II}} r_1) = \mu_n^{\mathrm{II}}(K_1(\mu_n^{\mathrm{II}} r_2)\mathrm{I}_1(\mu_n^{\mathrm{II}} r_1) - \mathrm{I}_1(\mu_n^{\mathrm{II}} r_2) K_1(\mu_n^{\mathrm{II}} r_1))$$

The functions $\mathrm{I}_v(z)$ and $K_v(z)$ are the modified Bessel functions of the first and second kind respectively of order v.

REFERENCES

Aller, R. C. (1978). Experimental studies of changes produced by deposit feeders on pore water, sediment, and overlying water chemistry. *Am. J. Sci.*, **278**, 1185–1234.

Aller, R. C. (1980). Quantifying solute distributions in the bioturbated zone of marine

sediments by defining an average microenvironment. *Geochim. Cosmochim. Acta*, **44**, 1955–65.

Aller, R. C. (1982). The effects of macrobenthos on chemical properties of marine sediment and overlying water. In: McCall, P. L., and Tevesz, M. J. S. (eds), *Animal–Sediment Relations*, pp. 53–102. Plenum Press, New York.

Aller, R. C. (1983). The importance of the diffusive permeability of animal burrow linings in determining marine sediment chemistry. *J. Mar. Res.*, **41**, 299–322.

Aller, R. C. (1984). The importance of relict burrow structures and burrow irrigation in controlling sedimentory solute distributions. *Geochim. Cosmochim. Acta*, **48**, 1929–34.

Aller, J. Y. and Aller, R. C. (1986). Evidence for localized enhancement of biological activity associated with tube and burrow structures in deep-sea sediments at the Hebble site, Western North Atlantic. *Deep-Sea Res.*, **33**, 755–90.

Aller, R. C., and Yingst, J. Y. (1978). Biogeochemistry of tube-dwellings: a study of the sedentary polychaete *Amphitrite ornata* (Leidy). *J. Mar. Res.*, **36**, 201–54.

Aller, R. C., and Yingst, J. Y. (1985). Effects of the marine deposit-feeders *Heteromastus filiformis* (polychaeta), *Macoma balthica* (Bivalvia), and *Tellina texana* (Bivalvia) on averaged sedimentary solute transport, reaction rates, and microbial distributions. *J. Mar. Res.*, **43**, 615–45.

Aller, R. C., Yingst, J. Y., and Ullman, W. J. (1983). Comparative biogeochemistry of water in intertidal *Onuphis* (polychaeta) and *Upogebia* (crustacea) burrows: temporal patterns and causes. *J. Mar. Res.*, **41**, 571–604.

Aller, R. C., Mackin, J. E., Ullman, W. J., Wang, C-H, Tsai, S-M., Jin, J-C. Sui Y-N. and Hong, J-Z. (1985). Early chemical diagenesis, sediment–water solute exchange, and storage of reactive organic matter near the mouth of the Chang Jiang, East China Sea. *Cont. Shelf Res.*, **4**, 227–51.

Andrews, D., and Bennett, A. (1981). Measurements of diffusivity near the sediment-water interface with a finescale resistivity probe. *Geochim. Cosmochim. Acta*, **45**, 2169–76.

Berner, R. A. (1980). *Early Diagenesis: a theoretical approach*. Princeton University Press, Princeton, NJ.

Billen, G. (1978). A budget of nitrogen recycling in North Sea sediments off the Belgian coast. *Est. Coast. Mar. Sci.*, **7**, 127–46.

Billen, G. (1982). An idealized model of nitrogen recycling in marine sediments. *Am. J. Sci.*, **282**, 512–41.

Blackburn, T. H., and Henriksen, K. (1983). Nitrogen cycling in different types of sediments from Danish waters. *Limnol. Oceanogr.*, **28**, 477–93.

Boudreau, B. P. (1984). On the equivalence of nonlocal and radial-diffusion models for porewater irrigation. *J. Mar. Res.*, **42**, 731–5.

Bowden, W. B. (1984). A nitrogen-15 isotope dilution study of ammonium production and consumption in a marsh sediment. *Limnol. Oceanogr.*, **29**, 1004–15.

Boynton, W. R., Kemp, W. M., Osborne, C. G., Kaymeyer, K. R., and Jenkins, M. C. (1981). Influence of water circulation rate on *in situ* measurements of benthic community respiration. *Mar. Biol.*, **65**, 185–90.

Broecker, W. S., and Peng, T. H. (1974). Gas exchange rates between air and sea. *Tellus*, **26**, 21–35.

Chatarpaul, L., Robinson, J. B., and Kaushik, N. K. (1979). Role of tubificid worms in nitrogen transformations in stream sediments. *J. Fish. Res. Bd. Can.*, **36**, 673–8.

Chatarpaul, L., Robinson, J. B., and Kaushik, N. K. (1980). Effects of tubificid worms on denitrification and nitrification in stream sediment. *J. Fish. Res. Bd. Can.*, **37**, 656–63.

Emerson, S., Jahnke, R., Bender, M., Froelich, P., Klinkhammer, G., Bowser, C., and Sellock, G. (1980). Early diagenesis in sediments from the eastern equatorial Pacific. I. Pore water nutrient and carbonate results. *Earth Planet. Sci. Lett.*, **49**, 57–80.

Emerson, S., Jahnke, R., and Heggie, D. (1984). Sediment-water exchange in shallow water estuarine sediments. *J. Mar. Res.*, **42**, 709–30.

Fisher, J. B. (1982). Effects of macrobenthos on the chemical diagenesis of freshwater sediments. In: McCall, P. L., and Tevesz, M. J. S. (eds), *Animal–Sediment Relations*, pp. 177–218. Plenum Press, New York.

Focht, D. D., and Verstraete, W. (1977). Biochemical ecology of nitrification and denitrification. *Adv. Microbiol. Ecol.*, **1**, 135–214.

Froelich, P. N., Klinkhammer, G. P., Bender, M. L., Luedtke, N. A., Heath, G. R., Cullen, D., Dauphin, P., Hammond, D., Hartman, B., and Maynard, V. (1979). Early oxidation of organic matter in pelagic sediments of the eastern equatorial Atlantic: suboxic diagenesis. *Geochim. Cosmochim. Acta*, **43**, 1075–91.

Greenwood, D. J. (1968). Measurement of microbial metabolism in soil. In: Gray, T. R. G., and Parkinson, D. (eds), *The Ecology of Soil Bacteria*, pp. 138–57. University of Toronto Press.

Grundmanis, V., and Murray, J. W. (1982). Aerobic respiration in pelagic marine sediments. *Geochim. Cosmochim. Acta*, **46**, 1101–20.

Hargrave, B. T. (1970). The effect of a deposit-feeding amphipod on the metabolism of benthic microflora. *Limnol. Oceanogr.*, **15**, 21–30.

Hargrave, B. T. (1976). The central role of invertebrate faeces in sediment decomposition. In: Anderson, J. M., and Macfayden, A. (eds), *The Role of Terrestrial and Aquatic Organisms in Decomposition Processes*. Proc. Symp. Brit. Ecol. Soc., 17, pp. 301–21.

Hargrave, B. T., and Philips, G. A. (1977). Oxygen uptake of microbial communities on solid surfaces. In: Cairns, J., Jr (ed.), *Aquatic Microbial Communities*. Garland, New York.

Hattori, A. (1983). Denitrification and dissimilatory nitrate reduction. In: Carpenter, E. J., and Capone, D. G. (eds), Nitrogen in the Marine Environment, pp. 191–232. Academic Press, New York.

Henriksen, K., Hansen, J. I., and Blackburn, T. H. (1980). The influence of benthic infauna on exchange rates of inorganic nitrogen between sediment and water. *Ophelia*, Suppl. 1, 249–56.

Henriksen, K., Hansen, J. I., and Blackburn, T. H. (1981). Rates of nitrification, distribution of nitrifying bacteria, and nitrate fluxes in different types of sediment from Danish waters. *Mar. Biol.*, **61**, 299–304.

Henriksen, K., Rasmussen, M. B., and Jensen, A. (1983). Effect of bioturbation on microbiol nitrogen transformations in the sediment and fluxes of ammonium and nitrate to the overlying water. *Ecol. Bull. (Stockholm)*, **35**, 193–205.

Hylleberg, J. (1975). Selective feeding by *Aberenicola pacifica* with notes on *Abarenicola vagabunda* and a concept of gardening in lugworms. *Ophelia*, **14**, 113–37.

Hylleberg, J., and Henriksen, K. (1980). The central role of bioturbation in sediment mineralization and element recycling. *Ophelia*, Suppl. 1, 1–16.

Jahnke, R., Emerson, S., and Murray, J. W. (1982). A model of oxygen reduction, denitrification, and organic matter mineralization in marine sediments. *Limnol. Oceanogr.*, **27**, 610–23.

Jenkins, M. C., and Kemp, W. M. (1984). The coupling of nitrification and denitrification in two estuarine sediments. *Limnol. Oceanogr.*, **29**, 609–19.

Jørgensen, B. B., and Revsbech, N. P. (1985). Diffusive boundary layer and the oxygen uptake of sediments and detritus *Limnol. Oceanogr.*, **30**, 111–22.

Kaplan, W. A. (1983). Nitrification. In: Carpenter, E. J., and Capone, D. G. (eds), *Nitrogen in the Marine Environment*, pp. 139–90. Academic Press, New York.

Kaspar, H. F. (1982). Denitrification in marine sediment: measurement of capacity and estimate of *in situ* rate. *Appl. Environ. Microbiol.*, **43**, 522–7.

Kaspar, H. F. (1983). Denitrification, nitrate reduction to ammonium, and inorganic nitrogen pools in intertidal sediments. *Mar. Biol.*, **74**, 133–9.

Kemp, W. M., Wetzel, R. L., Boynton, W. R., D'Elia, C. F., and Stevenson, J. C. (1982). Nitrogen cycling and estuarine interfaces: some current concepts and research directions. In: Kennedy, V. (ed.), *Estuarine Comparisons*, pp. 209–30. Academic Press, New York.

Klump, J. V., and Martens, C. S. (1983). Benthic nitrogen regeneration. In: Carpenter, E. J., and Capone, D. G. (eds), *Nitrogen in the Marine Environment*, pp. 411–57. Academic Press, New York.

Koike, I., and Hattori, A. (1978). Denitrification and ammonia formation in anaerobic coastal sediments. *Appl. Environ. Microbiol.*, **35**, 278–82.

Kristensen, E. (1983). Ventilation and oxygen uptake by three species of *Nereis* (Annelida: Polychaeta). I. Effects of hypoxia. *Mar. Ecol. Prog. Ser.*, **12**, 289–97.

Kristensen, E. (1984). Effect of natural concentrations on nutrient exchange between a polychaete burrow in estuarine sediment and the overlying water. *J. Exp. Mar. Biol. Ecol.*, **75**, 171–90.

Kristensen, E., Jensen, M. H., and Andersen, T. K. (1985). The impact of polychaeta (*Nereis virens* Sars) burrows on nitrification and nitrate reduction in estuarine sediments. *J. Exp. Mar. Biol. Ecol.*, **85**, 75–91.

Lerman, A. (1979). *Geochemical Processes: water and sediment environments*. John Wiley & Sons, New York.

Li, Y.-H., and Gregory, S. (1974). Diffusion of ions in sea water and in deep-sea sediments. *Geochim. Cosmochim. Acta*, **38**, 703–14.

Liu, K.-K., and Kaplan, I. R. (1984). Denitrification rates and availability of organic matter in marine environments. *Earth Planet Sci. Lett.*, **68**, 88–100.

Matisoff, G., Fisher, J. B., and Matis, S. (1985). Effects of benthic macroinvertebrates on the exchange of solutes between sediments and fresh water. *Hydrobiologia*, **122**, 19–33.

Nixon, S. W., Oviatt, C. A., and Hale, S. S. (1976). Nitrogen regeneration and the metabolism of coastal marine bottom communities. In: Anderson, J. M., and MacFadyed, A. (eds), *The Role of Terrestrial and Aquatic Organisms in Decomposition Processes*, pp. 269–83. Proc. 17th Symposium, Brit, Ecol. Soc. Blackwell, Oxford.

Reise, K. (1981). High abundance of small zoobenthos around biogenic structures in tidal sediments of the Wadden Sea. *Helgolander Mecresunters*, **34**, 413–25.

Revsbach, N. P., Sørensen, J., Blackburn, T. H., and Lomholt, J. P. (1980). Distribution of oxygen in marine sediments measured with microelectrodes. *Limnol. Oceanogr.*, **25**, 403–11.

Rhoads, D. C. (1974). Organism–sediment relations on the muddy sea floor. *Oceanogr. Mar. Biol. Ann. Rev.*, **12**, 263–300.

Robbins, J. A. (1986). A model for particle selective transport of tracers in sediments with conveyor belt deposit feeders. *J. Geophys. Res.*, **91**, 8542–58.

Sayama, M., and Kurihara, Y. (1983). Relationship between activity of the polychaetous annelid, *Neanthes japonica* (Izuka) and nitrification-denitrification processes in the sediments. *J. Exp. Mar. Biol. Ecol.*, **72**, 233–42.

Seitzinger, S. P., Nixon, S. W., and Pilson, M. E. Q. (1984). Denitrification and nitrous oxide production in a coastal marine ecosystem. *Limnol. Oceanogr.*, **29**, 73–83.

Skopintsev, B. A. (1981). Decomposition of organic matter of plankton, humification, and hydrolysis. In: Duursma, E. K., and Dawson, R. (eds), *Marine Organic Chemistry: evolution, composition, interactions, and chemistry of organic matter in sea water*, pp. 125–77. Elsevier, New York.

Stefanson, R. C. (1972). Soil denitrification in sealed soil–plant systems. II. Effect of disturbed and undisturbed soil samples. *Plant Soil*, **37**, 141–9.

Sørensen, J. (1978). Capacity for denitrification and reduction of nitrate to ammonia in a coastal marine sediment. *Environ. Microbiol.*, **35**, 301–5.

Thayer, C. W. (1983). Sediment-mediated biological disturbance and the evolution of marine benthos. In: Tevesz, M. J. S., and McCall, P. L. (eds), *Biotic Interactions in Recent and Fossil Benthic Communities*, pp. 480–625. Plenum, New York.

Thompson, R. K. (1972). Functional morphology of the hind-gut gland of *Upogebia pugettensis* (Crustacea, Thalassinidia) and its role in burrow construction. Ph.D. dissertation, University of California, Berkeley.

Ullman, W. J., and Aller, R. C. (1982). Diffusion coefficients in nearshore marine sediments. *Limnol. Oceanogr.*, **27**, 552–6.

Vanderborght, J. P., and Billen, G. (1975). Vertical distribution of nitrate in interstitial water of marine sediments with nitrification and denitrification. *Limnol. Oceanogr.*, **20**, 953–61.

Waslenchuk, D. G., Matson, A., Zajac, R. N., Dobbs, F. C., and Tramontano, J. M. (1983). Geochemistry of burrow waters vented by a bioturbating shrimp in Bermudian sediments. *Mar. Biol.*, **72**, 219–25.

Westrich, J. T., and Berner, R. A. (1984). The role of sedimentary organic matter in bacterial sulfate reduction: the G model tested. *Limnol. Oceanogr.*, **29**, 236–49.

Yingst, J. Y., and Rhoads, D. C. (1980). The role of bioturbation in the enhancement of microbial turnover rates in marine sediments. In: Tenore, K. R., and Coull, B. C. (eds), *Marine Benthic Dynamics*, pp. 407–22. University of South Carolina Press.